

Numerical investigation on strengthening steel beams with web openings using GFRP

Hamda Guedaoura, Yazid Hadidane

Civil Engineering Laboratory (LGC), Badji Mokhtar- Annaba University, P. O. Box 12, 23000 Annaba, Algeria

hamda.guedaoura@gmail.com; hamda.guedaoura@univ-annaba.org

y.hadidane@gmail.com; yazid.hadidane@univ-annaba.dz

Mohammed J. Altaee

Environment research and studies center, University of Babylon, Hilla, Iraq

mohammed.altaee@uobabylon.edu.iq

ABSTRACT. This study presents the first investigation into the use of glass fiber reinforced polymer GFRP to strengthen steel beams with web openings. Based on previous research about the strengthening of steel beams with web perforation using carbon fiber reinforced polymer (CFRP) conducted by one of the contributing authors of this paper, it was decided to investigate the ability of pultruded glass fiber reinforced polymer, which is less expensive than CFRP materials, to strengthen single rectangular web openings of steel beams. The previous published experimental test was used to validate the proposed numerical model developed with the finite element software ABAQUS, capable of acquiring important phenomena such as debonding between FRP and steel material. The validated simulation was then used to operate a parametric study involving four proposed GFRP strengthening techniques and three distinct pultruded GFRP product thicknesses to reinforce the same steel beam used in the earlier experimental test, having a single rectangular opening shape in two separate positions along the span. From these numerical models, an adequate GFRP strengthening arrangement was found and the possibility of using low-modulus FRP materials rather than the more expensive high-modulus FRP materials for strengthening steel beams with web penetration was confirmed.



Citation: Guedaoura H., Hadidane, Y., Altaee, M., Numerical investigation on strengthening Steel Beams with web openings using GFRP, *Frattura ed Integrità Strutturale*, 62 (2022) 26-53.

Received: 17.06.2022

Accepted: 20.07.2022

Online first: 24.07.2022

Published: 01.10.2022

Copyright: © 2022 This is an open access article under the terms of the CC-BY 4.0, which permits unrestricted use, distribution, and reproduction in any medium, provided the original author and source are credited.

KEYWORDS. GFRP; Web openings; Strengthening; Finite element model; Failure modes.



INTRODUCTION

With the remarkable progress of modern technology in all areas of daily use, new houses use an automated process to automatically control the building's operation, including lighting, ventilation, water supply, PC system, security, and other systems to ensure a high level of comfort.

Certainly, the idea of converting an existing home to a smart home can be easier for homeowners than buying a new one. However, the addition of devices requires engineers and major companies to create openings in the web of existing steel beams for the placement of services and the laying of lines and cables.

Despite this operation having become an acceptable engineering practice, the presence of openings in the web affects the normal flow of stresses and their distribution in the beam, which leads to a reduction in the load-carrying capacity of the beam depending on the opening shape, size, and location along the span [1,2].

So it is evident that steel beams with web openings needed a strengthening process to compensate and restore their loss in stiffness and strength. The only strengthening technique in existing design rules for such beams is the welding of a steel plate above and below the opening [3,4]. Although several research works [5,6] confirmed the ability of this strengthening technique to recover the strength of the beam, the practical difficulties and drawbacks of welding operation for the strengthening of steel elements cannot be neglected[1]. For this reason, it was an inevitable challenge for thinking heads and structural engineers to find an alternate method for the strengthening of steel structures.

As a result of the successful utilization of fiber composite products in different fields, FRPs have been gradually inserted into civil infrastructure applications since the 1980s [7] as an excellent strengthening material due to its high tensile strength to weight ratio, its resistance against corrosion and many other advantages [8].

A significant amount of research has been conducted to investigate the effectiveness of strengthening structural steel members using FRP materials. A numerical and experimental study was conducted by Narmashiri K [9] on the flexural strengthening of eight steel I-beams using different types of CFRP plates. Ardalani G and al [10] strengthened six plate girders using different lengths of CFRP plates bonded on the bottom flange. In the same axis ten steel I-beams were strengthened by Deng and Lee[11] using different length and thickness of CFRP plates, they found that besides to the enhancement in the strength and the stiffness of all strengthened specimens, failure modes were sensitive to the type, length and thickness of CFRP plates.

On the other hand, glass fiber reinforced polymer GFRP, which is less expensive by around 5 to 25 times than carbon fiber reinforced polymer CFRP [12] is also used in some researches. Okeil A and al [13] developed the Strengthening-By-Stiffening technique by bonding two pultruded T-shaped GFRP profiles on the two sides of the end web panels of plate-girders. The results of this experimental and numerical investigation showed a gain of 40% in the ultimate load compared to the unstiffened specimen. Another study was conducted by El Damatty and Abushagur [14] on the strengthening of a W steel-cross section beam using GFRP sheet bonded to the top and bottom flanges. Test results indicated an enhancement in the moment capacity of the beam. Accord N and al[15] found that the use of bonded GFRP strips in the compression flange of a steel I-shaped beam was able to increase the ductility of the member during plastic hinging.

It is clear from recent researches and many other published works in the last few years that FRP materials present an effective alternative means of strengthening for steel structures. However, it should be noted that debonding of FRP laminates was a dominant failure mode in most cases of studies, so it was necessary to understand the complex stress states that exist in the adhesive between FRP and steel. Particular importance was taken on evaluating the bond strength and bond behavior between FRP and steel using different theoretical and experimental test methods [8]. Recently an advanced finite element approach was investigated by Fernando D[16] for the prediction of debonding failure in FRP-strengthened steel beams.

Most of these efforts have focused on the use of CFRP and GFRP materials to improve the strength and stability of solid steel beams without openings. Currently, very few works has been done for the strengthening of steel beams with web openings using FRP materials. The first successful numerical and full-scale experimental investigation was conducted by the contributing author of this paper, Altaee M and al [17, 18] which proved the ability of high-modulus CFRP laminates to recover the elastic strength of steel beams with large rectangular opening using the most effective strengthening system and an adequate CFRP length to prevent the premature debonding failure. Recently, non-linear finite element modelling was performed by Mustafa Sand Fathy E [19] to determine the effectiveness of strengthening steel beams with circular and rectangular opening shapes of different sizes under cyclic loading using normal modulus CFRP and low modulus BFRP. The most suitable reinforcement length and thickness for each case of opening have been described. An experimental investigation was carried out by Hamoud and al. [20] on seven shear-loaded steel-plated girders with diamond and square



web perforation shapes, strengthened using two types of CFRP configurations. Results indicated an enhancement of 9 to 21% in the ultimate shear load for strengthened specimens.

Since the strengthening of steel beams with web opening using FRP is a novel technique, to date there are no design guides or manuals to use for the construction industry. More elaborate investigations and other tests of different parameters are needed to provide sufficient information to make recommendations and fully understand the use of FRP-strengthening of web opening in existing steel beams. The idea of this study is to explore the ability of low modulus fibers (glass fibers) for the strengthening of steel I beams with web opening under static loading.

FINITE ELEMENT MODEL DESCRIPTION AND VALIDATION WITH PREVIOUS EXPERIMENTAL RELATED STUDY

This section of this research describes the finite element modeling that has been conducted using the software package ABAQUS in terms of solver type, material modeling, and material failure criterion[21–24].The proposed FE model was compared to the previous experimental test done by the collaborating author of this research, Altaee M and al[18], which consisted of simply supported 305x102x25 UKBs steel section beams with a 3 meter effective span. B0 is the basic solid specimen without a web opening, whereas B1-R0 and B2-R0 are CFRP reinforced specimens having individual rectangular web holes of 210 x 185mm in the mid span and shear regions, correspondingly. Specimens were loaded under a six-point flexure test to generate a uniformly distributed load and were laterally constrained in four sites along the beam span. The 3 mm CFRP plate has a 200 GPa elastic modulus and bonded using an epoxy glue with a 1.5 GPa Young's modulus and a tensile strength of 29 MPa. The effective bond length was equal to 840 mm. In Figs. 1 and 2, as well as Tab.1, Tab.2 and Tab.3 all configurations, dimensions, and material properties are given.

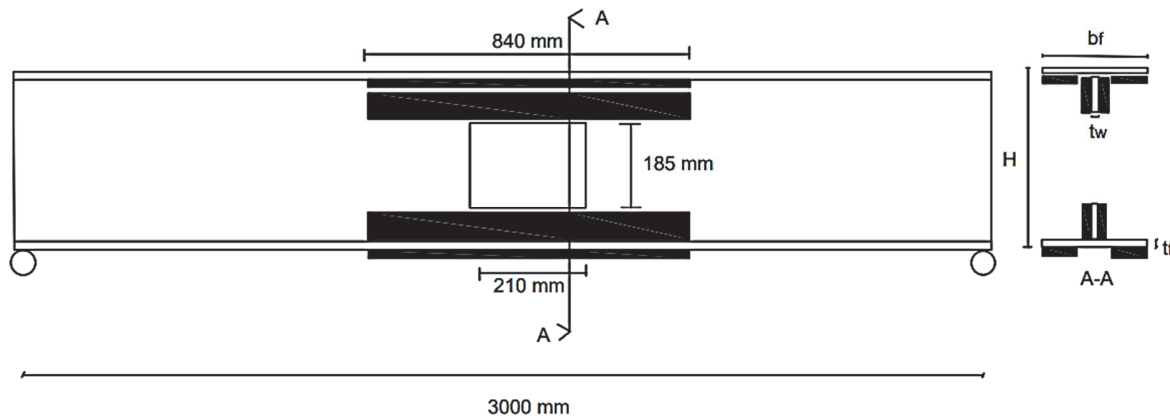


Figure 1: Details and dimensions of CFRP strengthened specimen B1-R0.

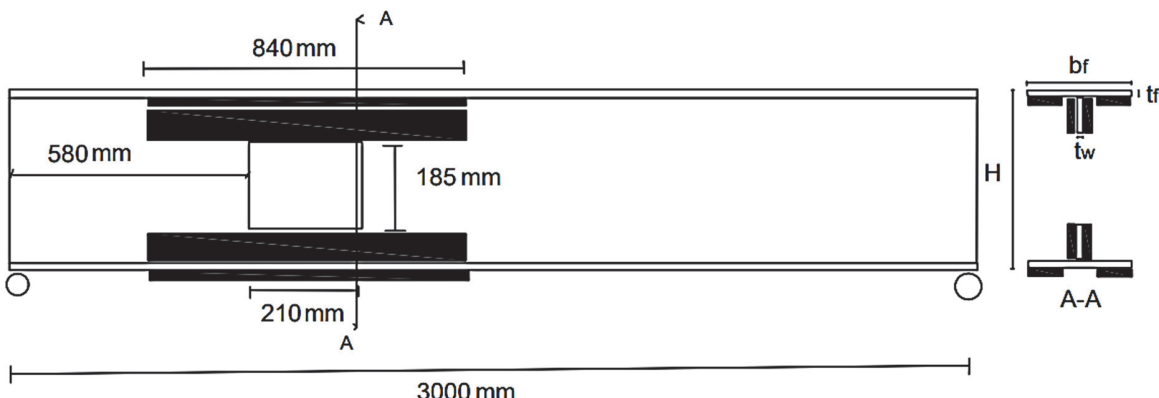


Figure 2: Details and dimensions of CFRP strengthened specimen B2-R0.

t_w (mm)	t_f (mm)	b_f (mm)	H (mm)	L (mm)	Web f_y (MPa)	Flange f_y (MPa)	Web E (GPa)	Flange E (GPa)
5.8	7	101.6	305.1	3000	435	412	210	206

Table 1: Tested specimens dimensions and steel properties.

E_x (MPa)	E_y (MPa)	E_z (MPa)	ν_{xy}	ν_{xz}	ν_{yz}	G_{xy} (MPa)	G_{xz} (MPa)	G_{yz} (MPa)
200000	14050	14050	0.29	0.29	0.6	5127.5	5127.5	4390.6

Table 2: Mechanical properties of HM CFRP.

Young's modulus (GPa)	Ultimate tensile strength (MPa)	Ultimate shear strength (MPa)	Strain at rupture %
1.5	29	26	4.6

Table 3: Mechanical properties of the adhesive.

Material modelling and Solver type

For better computational time, the Dynamic Explicit solver (ABAQUS/Explicit) was employed in this study which has been proved to be effective for solving certain quasi-static problems [25,26]. Since time has an influential role in dynamic analysis, the frequency analysis was first to find the suitable time for the expected failure mode. In addition to that, the smooth step function will be used to avoid the dynamic effects and high kinetic energies [26]. Both geometric and material nonlinearities are considered in this analysis. Steel was modeled as an isotropic material and the true stress-strain values were obtained using the following converting equations:

$$\varepsilon_{\text{true}} = \ln(\varepsilon_{\text{nominal}} + 1) \quad (1)$$

$$\sigma_{\text{true}} = \sigma_{\text{nominal}} (\varepsilon_{\text{nominal}} + 1) \quad (2)$$

The FRP composite material was classified as an orthotropic elastic [16]. Regarding the element type, a four-noded doubly curved shell element with reduced integration, S4R, was selected to model both steel and FRP laminates. The cohesive element COH3D8 was used as an element type of the adhesive [16,27].

Bond behaviour

To model an FRP-steel connection, the elastic range behavior and the adhesive degradation modelling for the mixed mode cohesive law will be detailed as:

Linear elastic traction-separation behaviour

Fig. 3 depicts the basic bilinear traction-separation assumption used in this study. Firstly, linear elastic behavior until the initiation of damage, then softening deviance that describes damage evolution. Thus, the interfacial performance before damage initiation can be defined by:

$$\begin{Bmatrix} t_n \\ t_s \\ t_t \end{Bmatrix} = \begin{bmatrix} K_{nn} & 0 & 0 \\ 0 & K_{ss} & 0 \\ 0 & 0 & K_{tt} \end{bmatrix} \begin{Bmatrix} \delta_n \\ \delta_s \\ \delta_t \end{Bmatrix} \quad (3)$$



The adhesive elastic stiffness in the normal direction is equivalent to the bond-separation model's initial slope for mode-I loading and can be represented as (Fig.3) [16]:

$$K_{nn} = \frac{E_a}{T_a} \quad (4)$$

The adhesive elastic stiffness in the shear direction, corresponds to the initial inclination of the bond-slip model which can be calculated from (Fig.3) [16]:

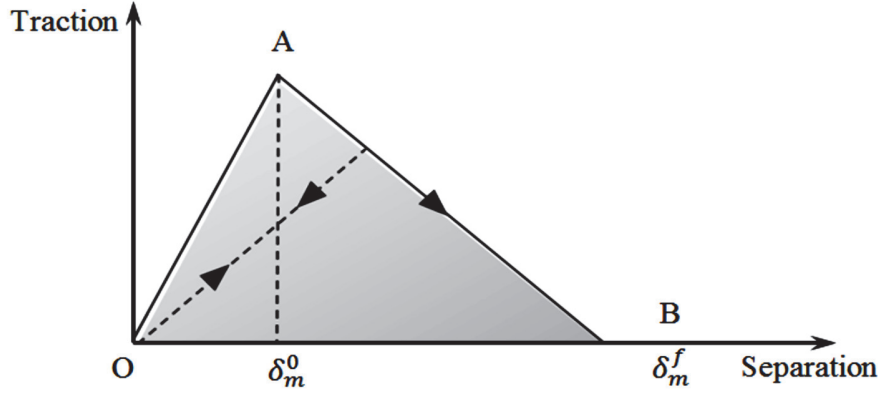


Figure 3: Simple bilinear traction-separation law [25].

$$K_{ss} = K_{tt} = 3 \left(\frac{G_a}{T_a} \right)^{0.65} \quad (5)$$

Damage initiation

In the present research, the quadratic nominal stress criterion provided in ABAQUS [25] is used for the interaction between mode-I and mode-II loading, which can be presented in Eqn. (6):

$$\left(\frac{\langle t_n \rangle}{\sigma_{max}} \right)^2 + \left(\frac{t_s}{\tau_{max}} \right)^2 + \left(\frac{t_t}{\tau_{max}} \right)^2 = 1 \quad (6)$$

The Macaulay bracket $\langle \rangle$ is used to signify that compressive stresses do not lead to damage.

Damage evolution

Following the damage initiation, a scalar degradation parameter, D, is employed, which is initially equal to 0 and uniformly progresses to 1 for the total damage of the bond interaction. It can be expressed by:

$$\begin{Bmatrix} t_n \\ t_s \\ t_t \end{Bmatrix} = \begin{bmatrix} (1-D^*)K_{nn} & 0 & 0 \\ 0 & (1-D)K_{ss} & 0 \\ 0 & 0 & (1-D)K_{tt} \end{bmatrix} \begin{Bmatrix} \delta_n \\ \delta_s \\ \delta_t \end{Bmatrix} \quad (7)$$

The damage index D can be expressed as:

$$D = \frac{\delta_m^f (\delta_m^{\max} - \delta_m^0)}{\delta_m^{\max} (\delta_m^f - \delta_m^0)} \quad (8)$$

Residual stresses and geometric imperfection

The model include an initial geometric imperfection based on the first buckling mode using Eigenvalue analysis. This imperfection is introduced with a scale factor of L/1000 [1], while in agreement with previous suggestions[7], residual stresses are not incorporated.

Mesh and boundary conditions

The chosen quadratic meshes of 25mm x 25mm from the mesh convergence study revealed satisfactory agreement in regards to stiffness, peak load, and load-deflection curves with experimental results. Regarding loading and boundary conditions of the experimental test lateral supports were dispersed over the beam length at 900mm c/c and the vertical load was directly applied to the beam in four point distributed along the top flange As illustrated in Fig.4. The specimens' extremities were mounted on two supports. The specimen was restricted vertically by both supports but was allowed to rotate. In the simulation model, the load and boundary conditions were applied precisely to the beam simultaneously to experimental test locations employing the rigid plates (Fig. 5). Two bearing plates were inserted into both ends of the specimens with the same features as in the experimental test. Hard interaction was performed as contact behavior with friction coefficients of 0.16 and 0.8 between the end support plates and the specimen, as well as between load plates and the specimen accordingly [17].

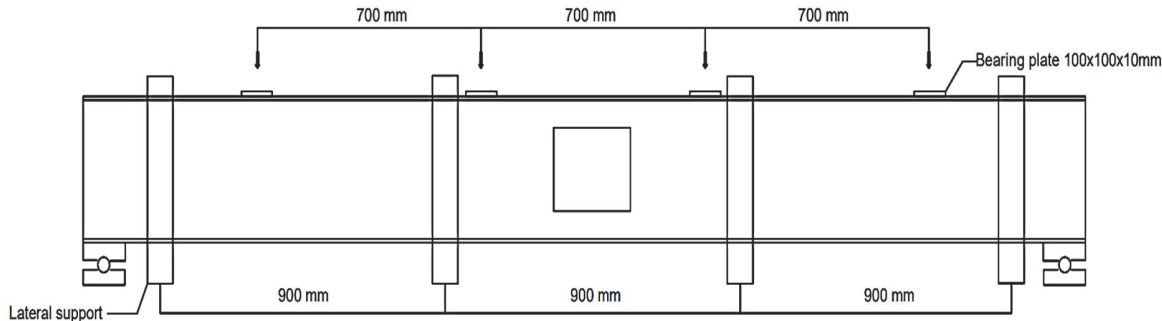


Figure 4: Experimental test arrangement.

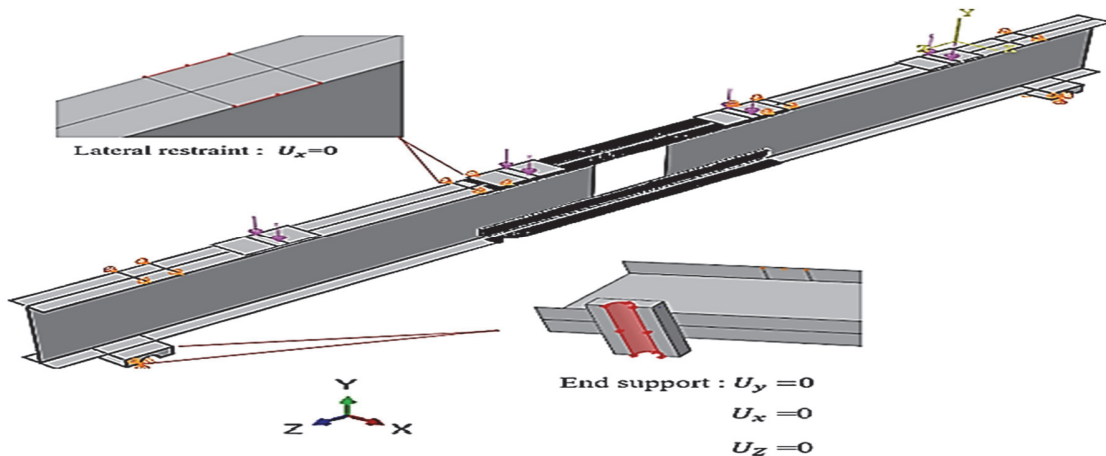


Figure 5: Details of loading and boundary conditions.

Finite element validation findings

As can be seen in Tab.4, the peak forces of studied specimens produced on the proposed finite element model were presented and compared to their related experimental results. The discrepancy in the ultimate load between the simulation model and the experimental test is less than 2% in all cases. For the three examined specimens, there was a close agreement between the finite element and experimental load-deflection curves (Fig.6). The failure mechanisms of tested specimens in FE models matched the findings of the experimental test (Tab.4). In the experimental test, the solid beam B0 failed by top flange yielding, which was accompanied by lateral torsional buckling. This was confirmed by the



simulation analysis (Fig.7). The specimens B1-RO and B2-RO failed also by top flange yielding followed by lateral torsional buckling far from the strengthened area. A similar failure mode was noticed in the finite element model (Figs. 8 and 9). Besides that, the numerical simulation indicated the debonding between CFRP and steel for specimen B1-RO employing the numerical parameter SDEG offered by ABAQUS[25], which starts at 0 and gradually increases to 1 for total bond interface damage. This is also proved by the deletion of the adhesive layer (Fig.10). The high degree of consistency between experimental and FE findings, as well as important test phenomena, provides confidence in using this proposed numerical model for reinforcing steel beams with web holes with glass fiber reinforced polymer GFRP rather than high modulus CFRP.

Specimen	$P_u(\text{exp})(\text{kN})$	$P_u(\text{FE})(\text{kN})$	$P_u(\text{exp})(\text{kN}) / P_u(\text{FE})(\text{kN})$	Failure mode
B0	406	407.14	0.997	TFY+LTB
B1-RO	488	492.04	0.991	TFY+LTB +DEB
B2-RO	424	426.32	0.994	TFY+LTB
Average			0.994	/

Table 4: Experimental and FE ultimate load comparison.

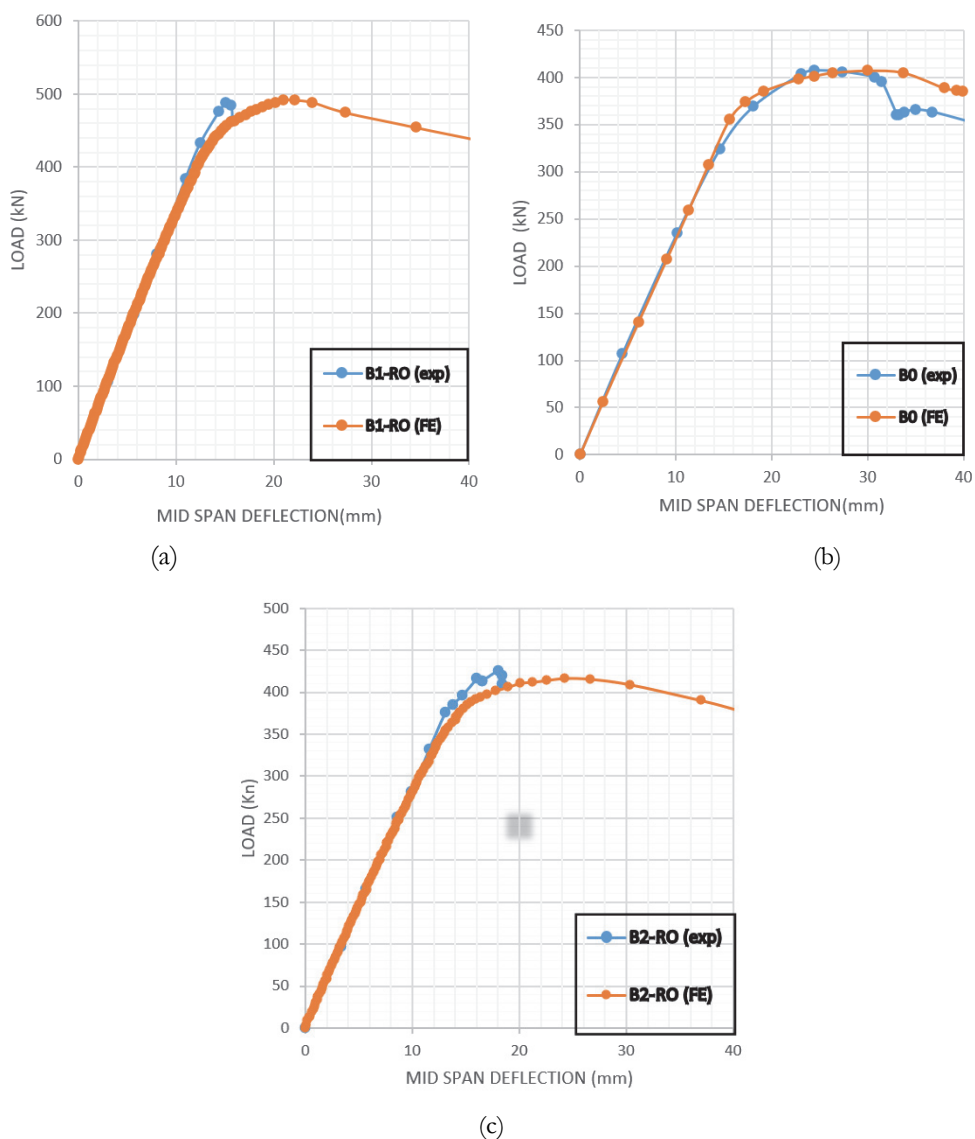


Figure 6: Load -deflection curves of specimens: (a) B0; (b) B1-RO;(c) B2-R0.

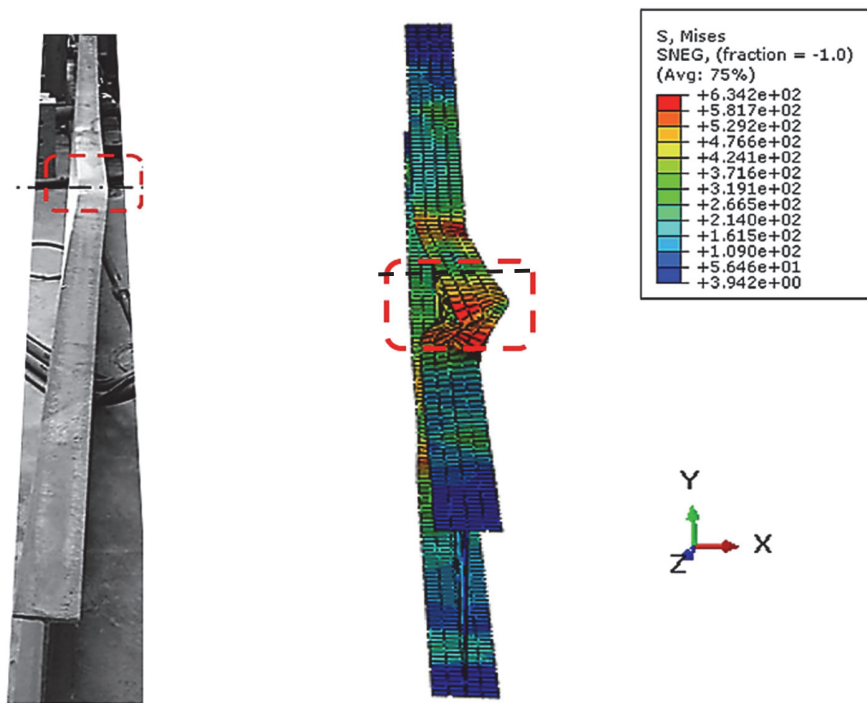


Figure 7: FE and experimental failure mode of specimen B0.

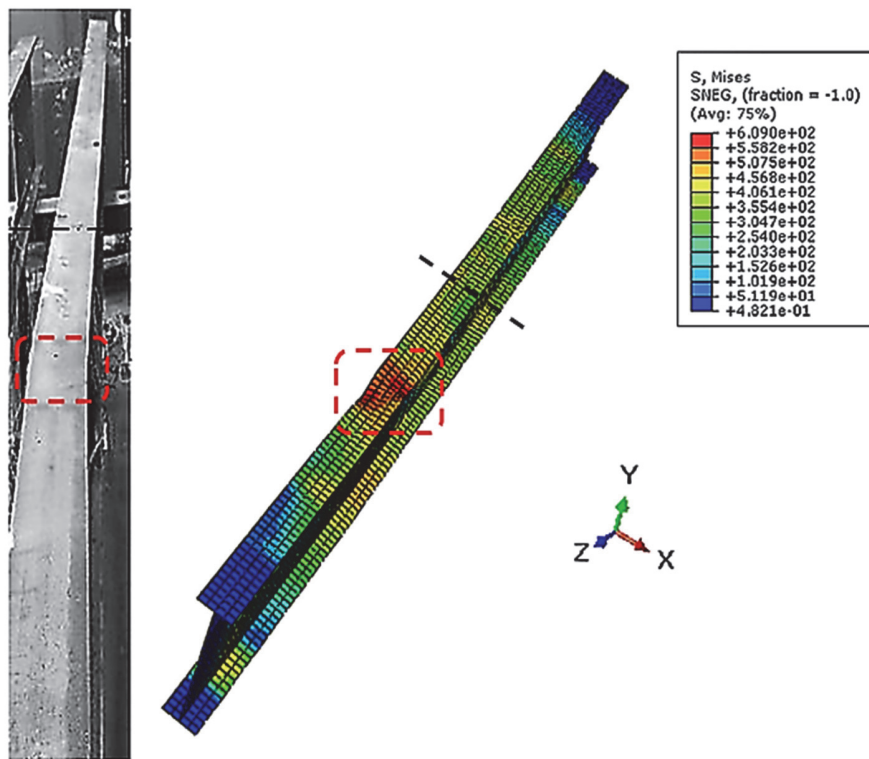


Figure 8: FE and experimental failure mode of specimen B1-R0.

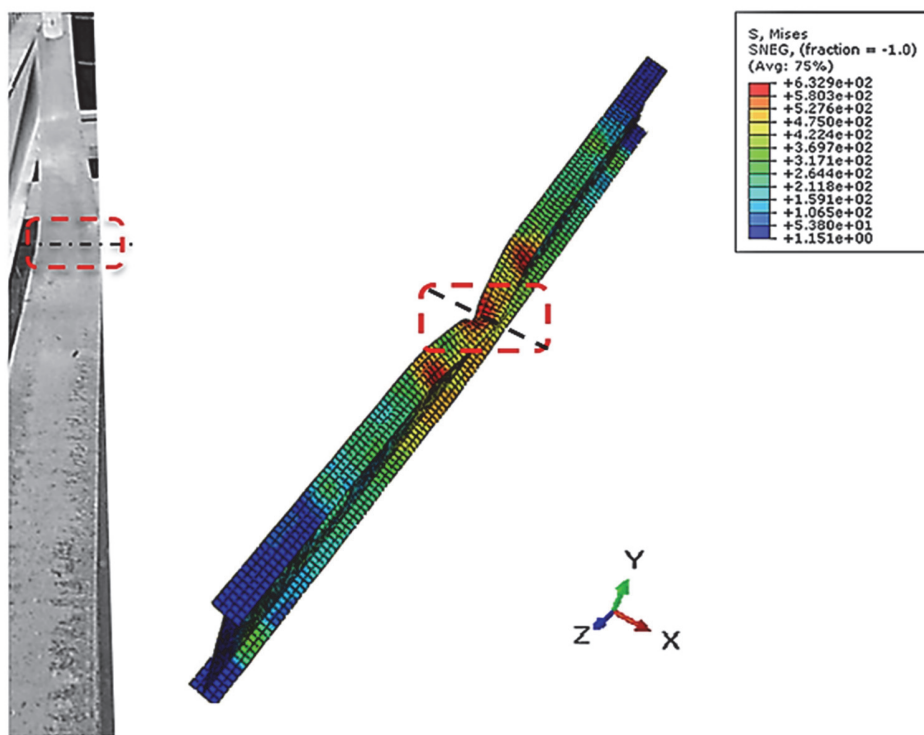


Figure 9: FE and experimental failure mode for specimen B2-R0.

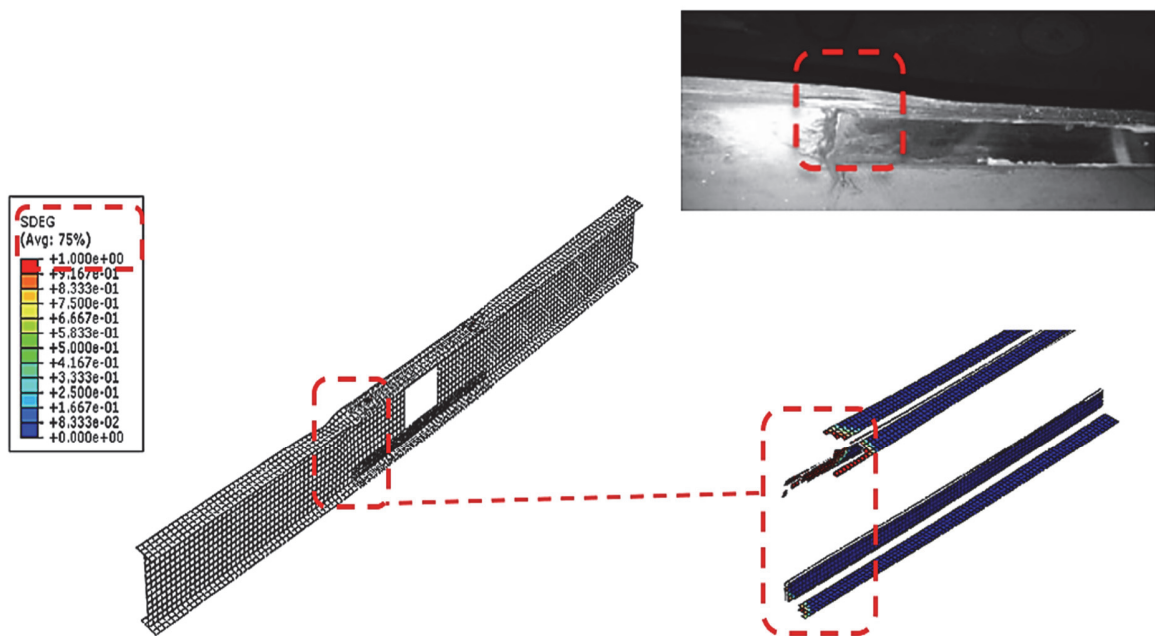


Figure 10: Experimental and FE Carbon FRP plate debonding for specimen B1-R0.

CASE STUDY

For more research credibility, using the validated numerical model, the verified specimen B0 was strengthened using pultruded GFRP laminates after the creation of rectangular web openings as in the previous study with the same opening dimensions and positions. The unstrengthened specimens with mid span and shear zone web openings were named B1-U0 and B2-U0, respectively. Four strengthening configurations were considered using pultruded GFRP plates and different GFRP profile shapes (U section–angle section–T section) (Figs.11 and 12) and (Tab.5). The GFRP elastic modulus was 18 GPa [28] (Tab.6). The adhesive and the bonding length were similar to the previous study. In addition, the influence of different GFRP laminate thicknesses was investigated.

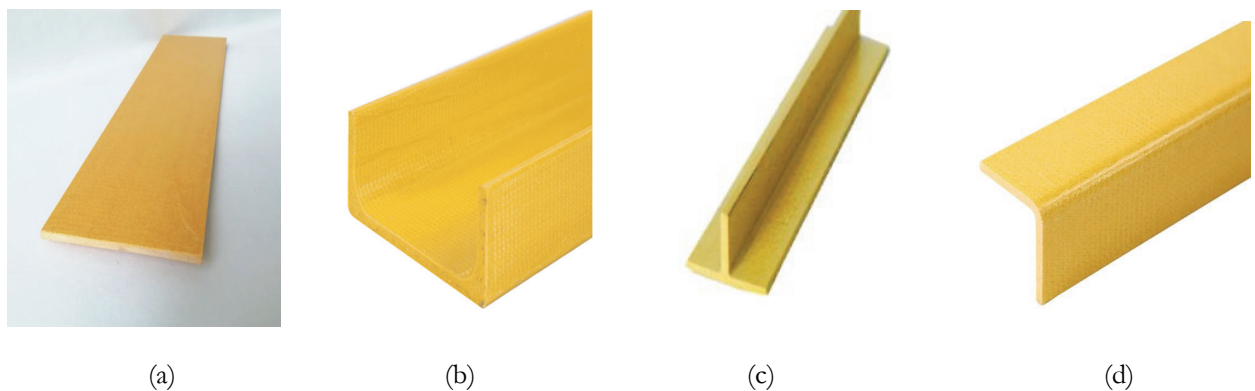


Figure 11: Pultruded GFRP : (a) Plate; (b)U section; (c) T section; (d) Angle section.

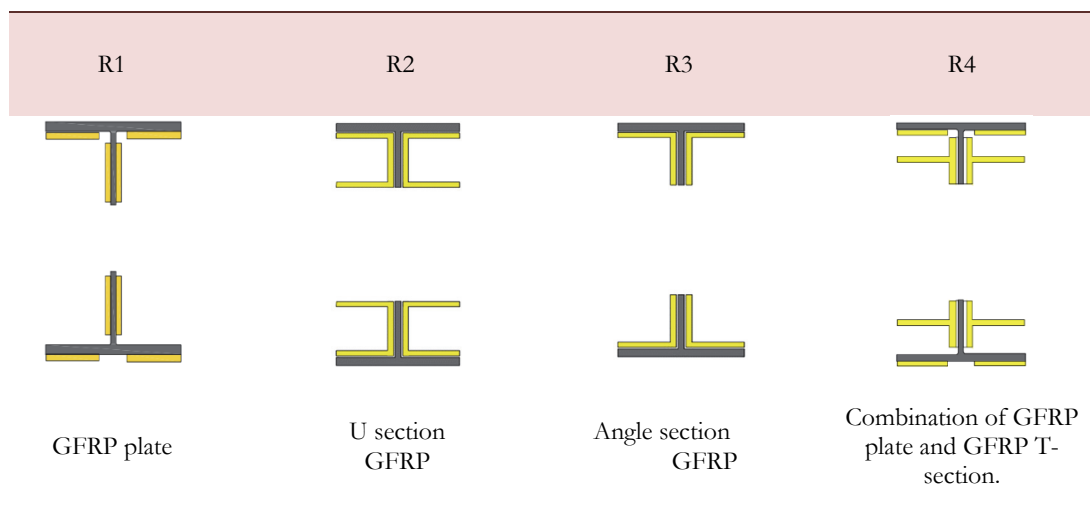


Table 5: The proposed GFRP strengthening configurations.

E_x (MPa)	E_y (MPa)	E_z (MPa)	ν_{xy}	ν_{xz}	ν_{yz}	G_{xy} (MPa)	G_{xz} (MPa)	G_{yz} (MPa)
18000	7000	7000	0.12	0.12	0.28	3000	3000	2750

Table 6: Mechanical properties of GFRP.

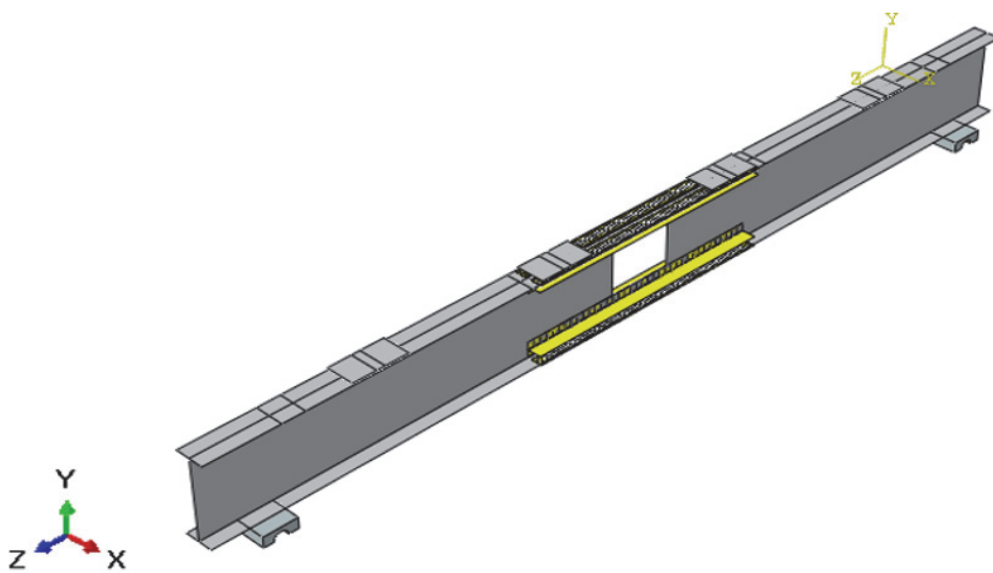


Figure 12: Strengthening specimen B1-U0 using (R4) GFRP technique.

The results will be discussed in regards to strength improvement, load-deflection response, failure mechanism, bond behavior, and will be compared to previous CFRP strengthening data.

RESULTS AND DISCUSSION

The following section describes the findings of the FE study. Every tested specimen was labeled: The first letter in every case identification is the designation of the tested beam, accompanied by the GFRP strengthening arrangement (R0-R1-R2-R3-R4), and eventually the GFRP laminate thicknesses (3mm-6mm-10mm). For example, "B1-R2-3" is the specimen B1 of mid span rectangular opening strengthened using R2 pattern with U GFRP sections of 3mm thicknesses.

Mid span position results

GFRP laminates of 3mm thicknesses

The creation of a rectangular web opening in the mid span of the beam resulted in a strength decrease of 12% compared to the initial beam B0, as shown by the load-deflection curve of specimen B1-U0 (Fig.13). Due to the presence of various GFRP strengthening patterns, different percentages of the strength and stiffness restore was noted in comparisons to the unstrengthened specimen B1-U0. The specimen B1-R1-3 showed an increase of 25 % in the strength enhancement, while specimens B1-R2-3 and B1-R3-3 were improved by 19%. Despite the strength of the solid beam B0 was recovered using R1, R2 and R3 strengthening configurations, only the "R4" reinforcement technique was able to exhibit the same strength enhancement found using CFRP in the previous study (B1-R0)[18], which was around 37 % compared to B1-U0 and 20 % over the solid beam B0. It was also observed that the stiffness of the original beam B0 was recovered in all cases of GFRP strengthened specimens, although it was not at the same level as the CFRP strengthened specimen B1-R0, which exhibited a stiffer response than the solid beam B0 (Fig.13). Specimens B1-R1-3, B1-R2-3, and B1-R3-3 demonstrated a very linear trend up to around 360 kN. of load. While for specimen B1-R4-3 the yielding load was around 380 kN. Further than this stress level, the commencement of plastic hinge generation was in the mid span above the opening. Consequently, lateral buckling was initiated in the beam's mid span (Figs.14 and 15). This was not the same failure mode as CFRP plates (Fig.8). Therefore, it can be noted that the adoption of 3 mm GFRP laminates did not impact the stress state of the beam. Regarding the bond behavior, the adhesive damage can be predicted from the simulation analysis, employing the numerical output parameter SDEG, which represents the adhesive's damage

progression. End debonding was started on the top flange of all GFRP reinforced specimens once the original force was attained. The SDEG parameter attained a value of 1, and the adhesive layer was deleted (Fig.16).

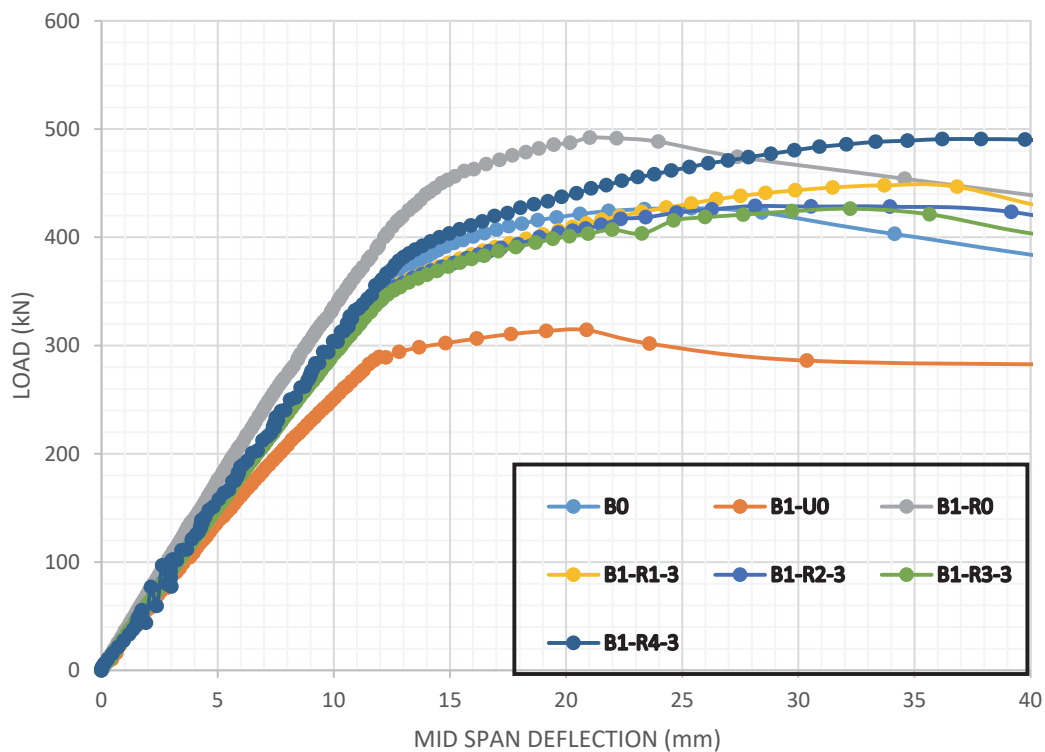


Figure 13: Load deflection curves of specimen B1-U0 strengthened using 3mm GFRP laminates thicknesses.

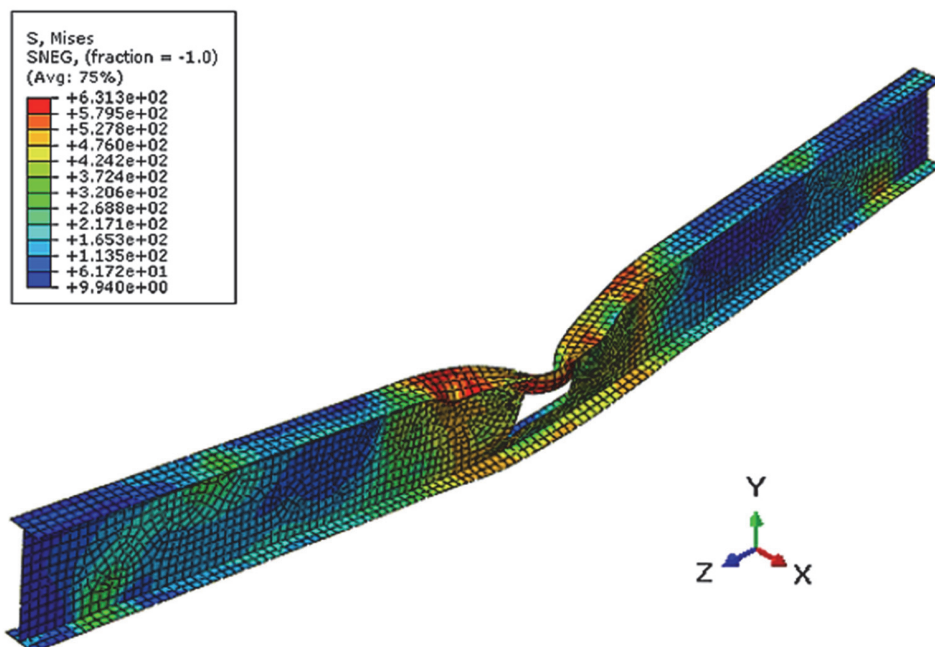


Figure 14: Mid span lateral buckling of specimen B1-R3-3.

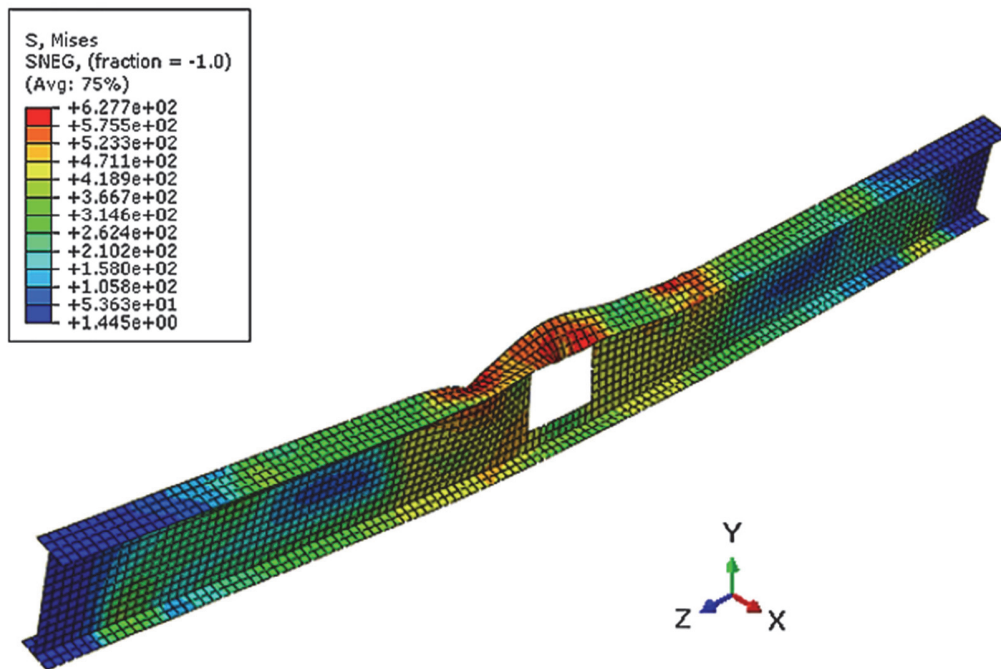


Figure 15: Mid span lateral buckling of specimenB1-R4-3.

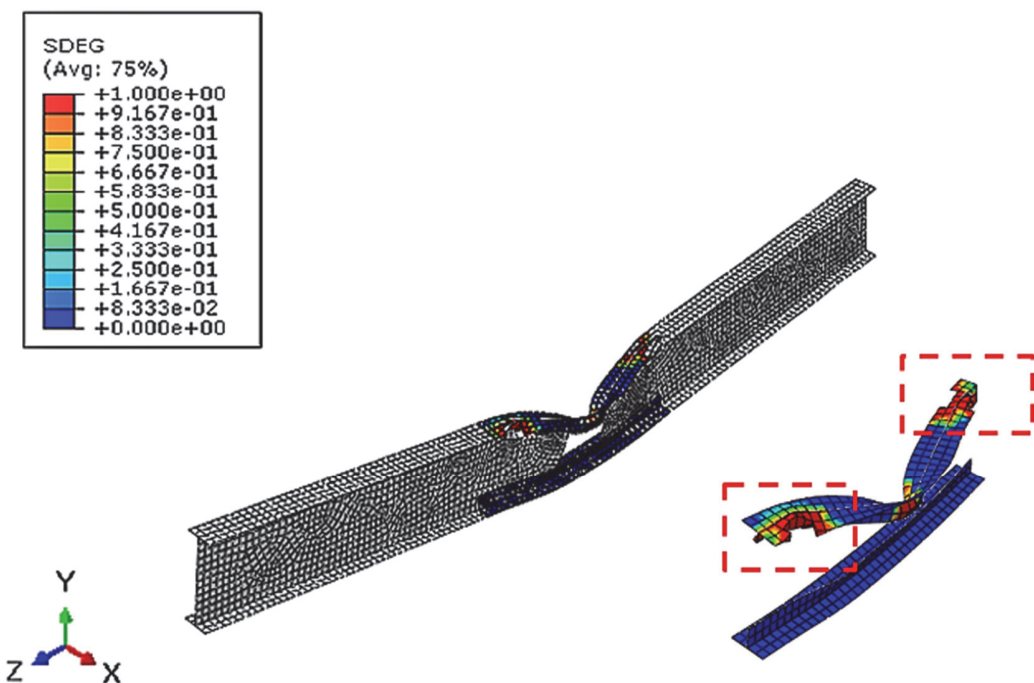


Figure 16: Bond behavior for specimen B1-R3-3.

GFRP laminates of 6mm thicknesses

Increasing the thickness of the GFRP laminates to 6mm allowed the reinforced specimens B1-R1-6, B1-R2-6, B1-R3-6, and B1-R4-6 to obtain a strength improvement percentage of 35%, 30%, 25%, and 43%, respectively, when compared to the unstrengthened beam B1-U0. As a result, all GFRP strengthened specimens with a thickness of 6 mm demonstrated a strength increase greater than the solid beam B0 (Fig.17). Besides that, the strength enhancement percentage of the 'R1' strengthening configuration with 6 mm plate thickness was comparable to 3mm CFRP plate strengthening (specimen B1-R0). Furthermore, the 'R4' strengthening pattern with 6 mm GFRP laminates provided a significant improvement in strength more than of the prior CFRP strengthening approach. However, even though the stiffness of the original beam B0 was restored with all 6mm GFRP strengthening cases, the specimen B1-R0 is considerably stiffer (Fig.17) and increasing the GFRP laminate thicknesses to 6mm did not really affect the stiffness in comparison to GFRP laminates of 3 mm thickness. B1-R1-6 and B1-R4-6 specimens showed a linear trend up to 360 kN and 380 kN of load, respectively. Further than this level of stress, the top flange at the end of the GFRP laminates saw the commencement of plastic hinge development. As a response, lateral buckling occurred far from the strengthened area at the end of the bonded GFRP laminates (Fig.18). This was the same failure mechanism as in the prior experiment, with the CFRP reinforcing arrangement [18]. On the other hand, specimens B1-R2-6 and B1-R3-6 demonstrated a very line graph up to around 350 kN. Above this load level, the top flange at the mid-span of the beam began to develop plastic hinges. Consequently, lateral buckling occurred in the mid span of the beam (Fig.19). Therefore, it should be stated that R2 and R3 strengthening designs with laminate thicknesses of 6 mm were unable to modify the failure mode of the examined specimens. In terms of bond behavior, end debonding of all GFRP reinforced specimens began at the top flange. Figs.20 and 21 shows that the SDEG indicator achieved a value of 1 at the adhesive end in specimens B1-R2-6 and B1-R3-6, confirming adhesive failure. As a result, the GFRP laminates were debonded there.

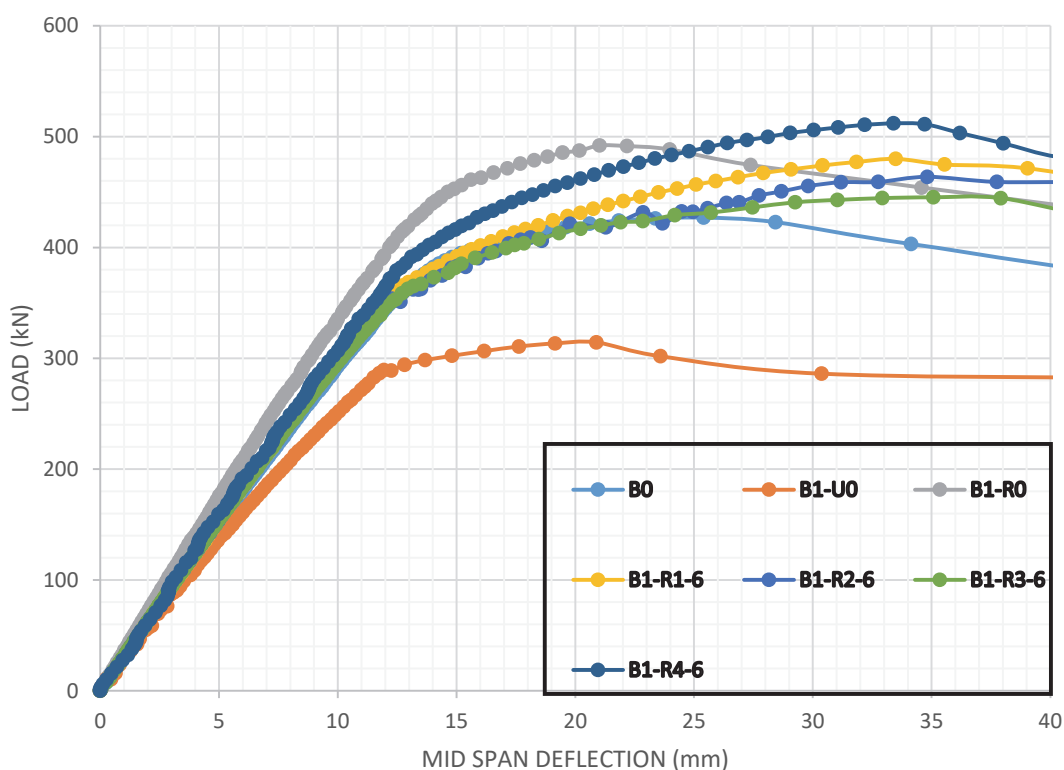


Figure 17: Load deflection curves of specimen B1-UO strengthened using 6 mm GFRP laminates thicknesses.

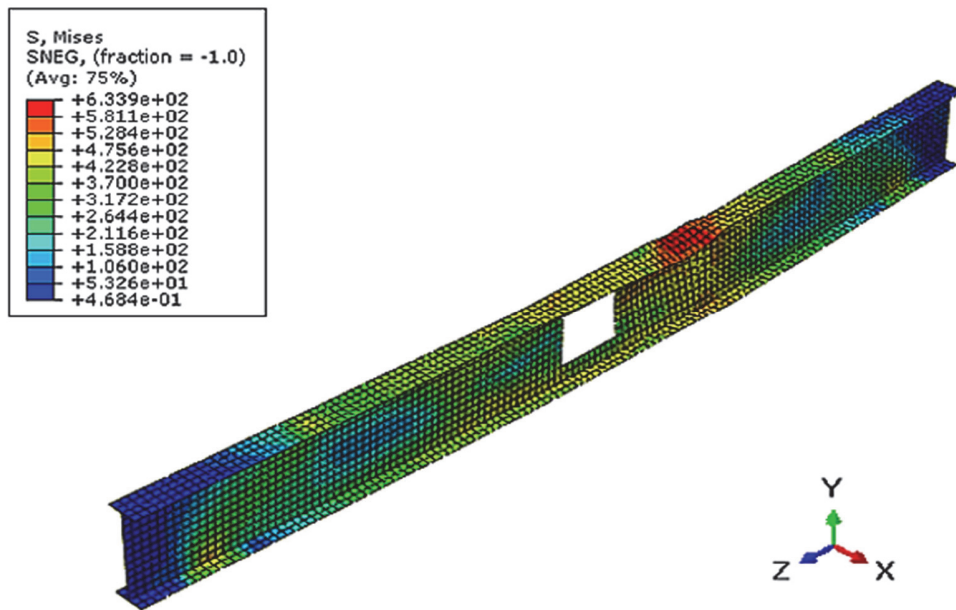


Figure 18: Failure mode of specimen B1-R4-6.

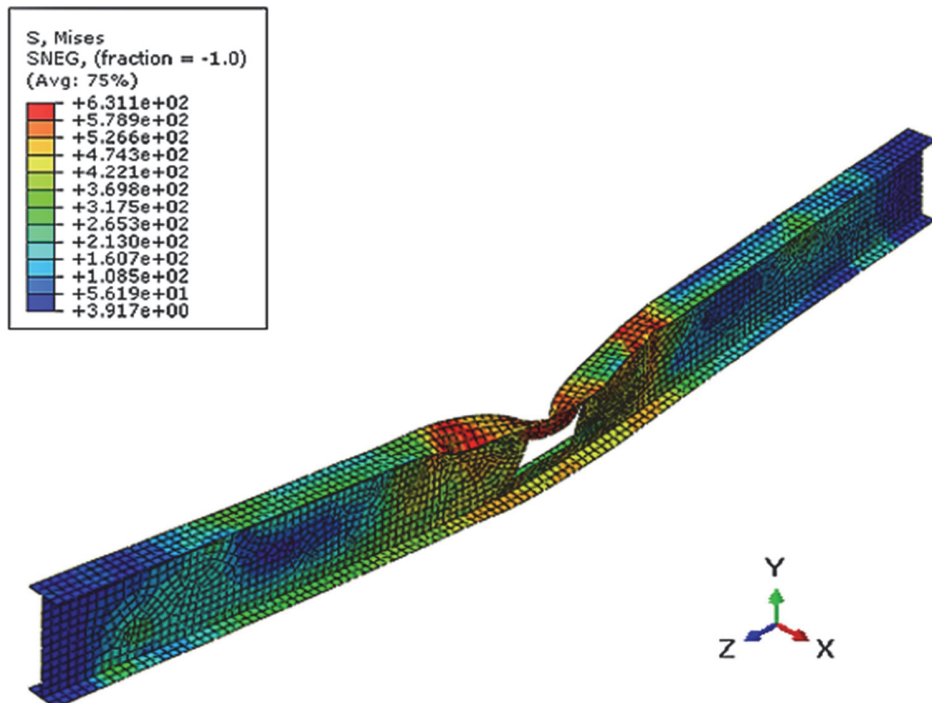


Figure 19: Failure mode of specimen B1-R3-6.

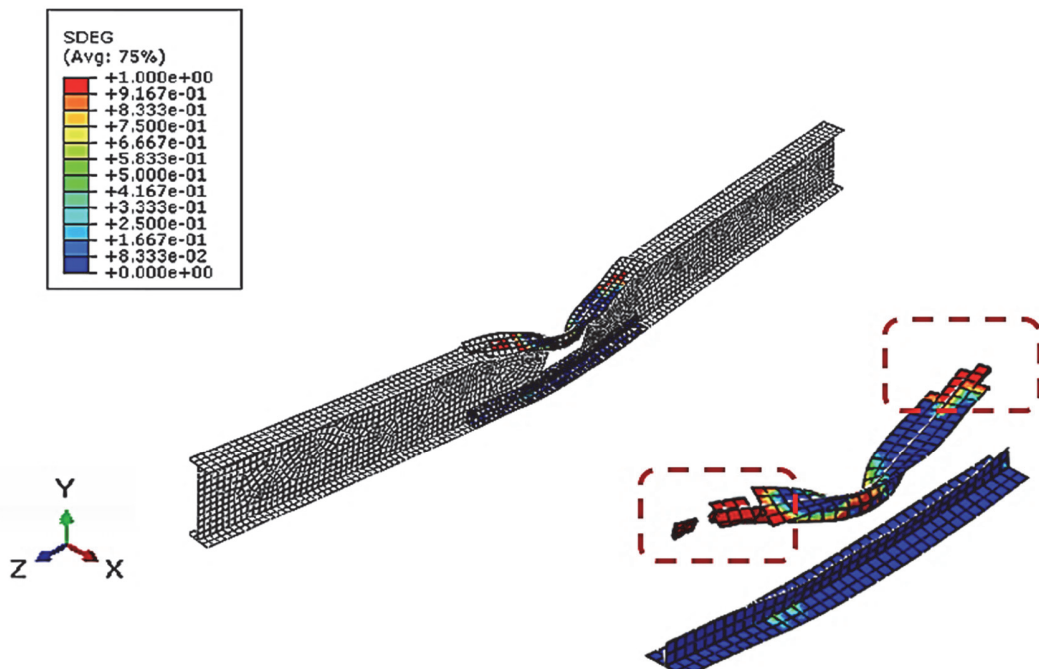


Figure 20: Bond behavior of specimen B1-R2-6.

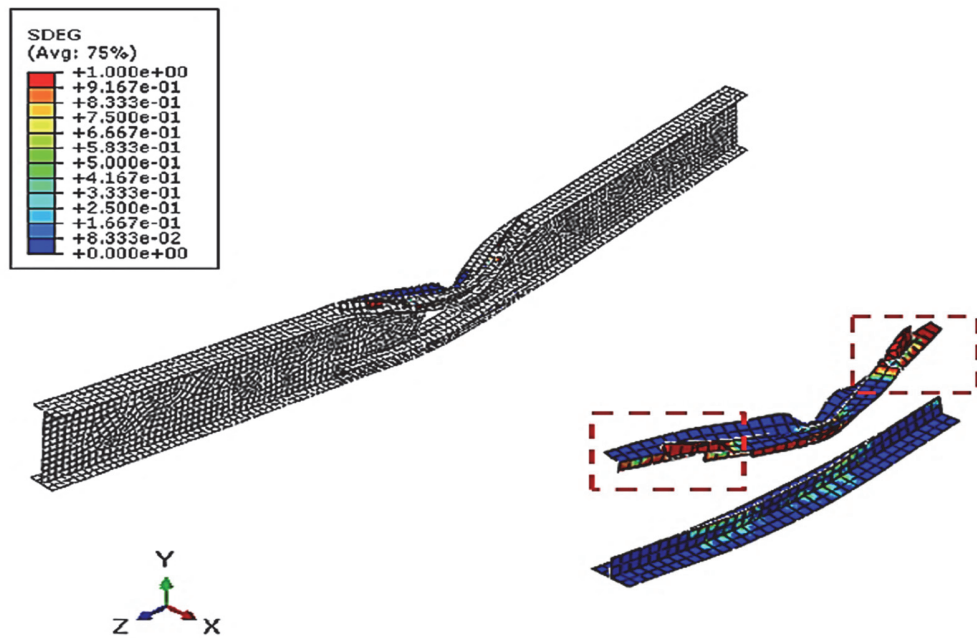


Figure 21: Bond behavior of specimen B1-R3-6.

GFRP laminates of 10 mm thicknesses

When the thicknesses of the GFRP laminates were increased to 10 mm, very intriguing results were observed. In contrast to B1-U0, specimens B1-R1-10, B1-R2-10, B1-R3-10, and B1-R4-10 improved in strength by 37 %, 33 %, 23 %, and 45



%, respectively. According to these numerical results, GFRP plates with a thickness of 10 mm ('R1') were able to achieve the same strength increase as CFRP plates with a thickness of 3 mm. Furthermore, utilizing the 'R4' configuration of 10 mm (B1-R4-10) revealed a 6% gain in strength over the prior CFRP strengthening with non-ductile response (Fig.22). Concerning stiffness, it is crucial to note that the original beam's stiffness was recovered using all strengthening patterns, with the 'R4' strengthening technique being the most comparable to the CFRP strengthening specimen (B1-R0) (Fig.22). Specimens B1-R1-10, B1-R2-10, and B1-R3-10 showed a linear curve up to the yielding load, which was about 365 Kn. Whereas specimen B1-R4-10 had a yielding load of 405 kN. Just above this load stage, the origins of plastic hinge initiation was observed at the end of the reinforcement zone. As a natural consequence, lateral buckling started at the end of GFRP laminates with top flange buckling for specimens B1-R1-10, B1-R2-10, and B1-R3-10 (Fig.23), while for specimen B1-R4-10 lateral buckling was not seen. The beam failed only by top flange buckling (Fig.24). This can be explained by the flexural stiffness of the T-section GFRP profile, which was able to prevent the out of plane buckling[29]. Brittle end debonding was observed (Fig.25) particularly specimen B1-R3-10. This demonstrates the significance of adjusting bond performance and laminate thickness. It appears to be plausible, the strength of the reinforced specimens will increase as the thickness of the GFRP laminates increases. However, the need for strength restoration must be controlled with the ductility response of the reinforced section and the bond performance to avoid premature debonding.

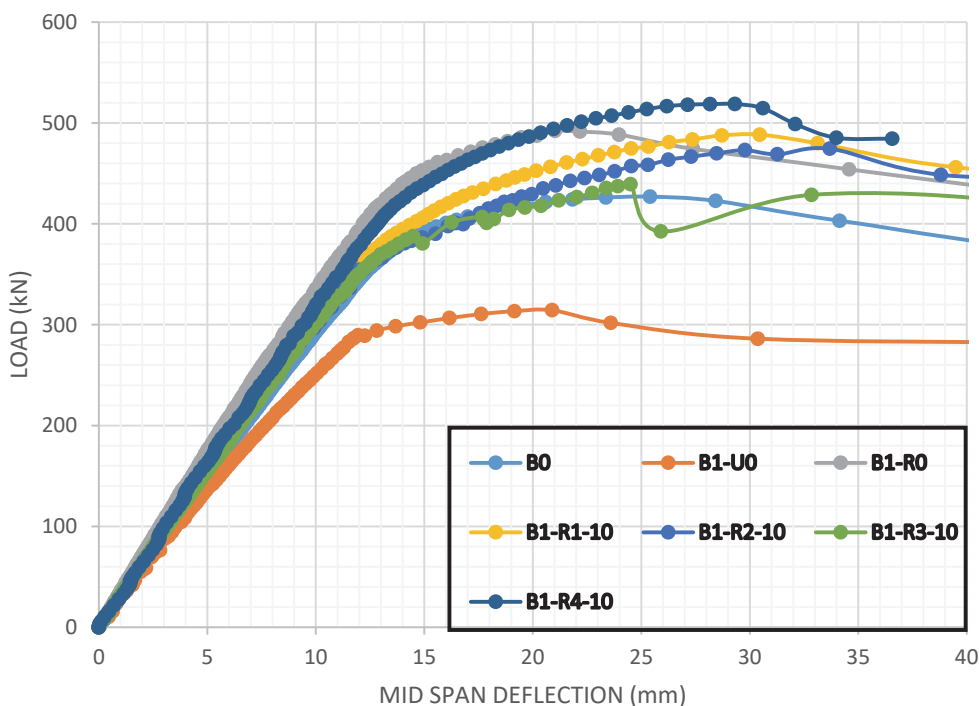


Figure 22: Load deflection curves of specimen B1-UO strengthened using 10 mm GFRP laminates thicknesses.

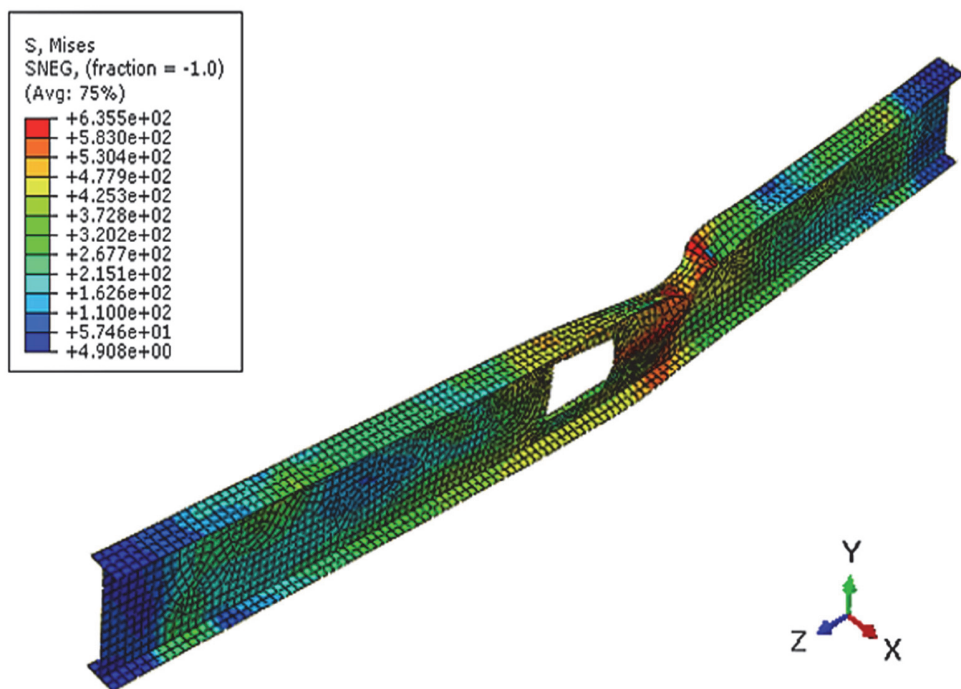


Figure 23: Failure mode of specimen B1-R1-10.

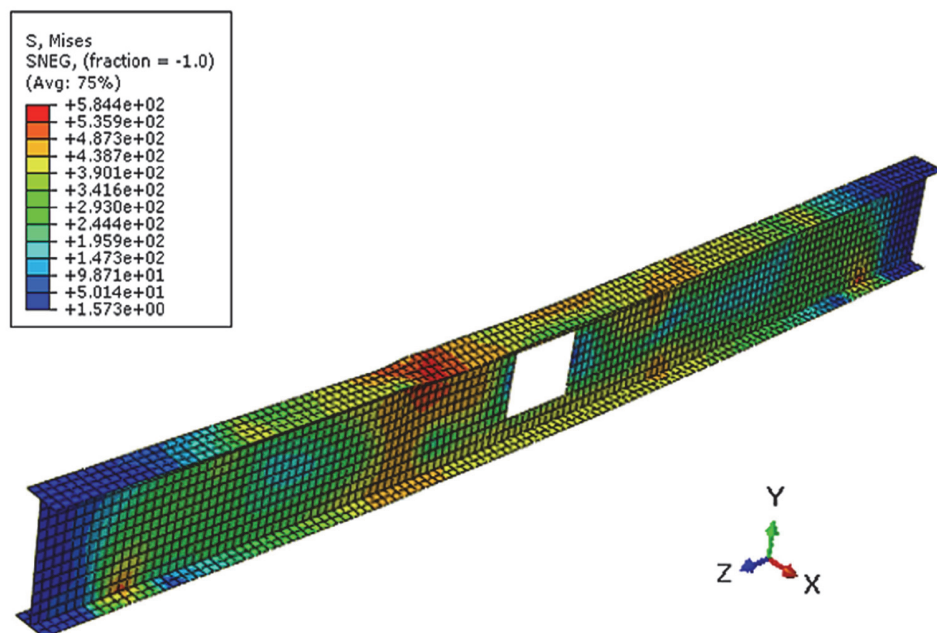


Figure 24: Failure mode of specimen B1-R4-10.

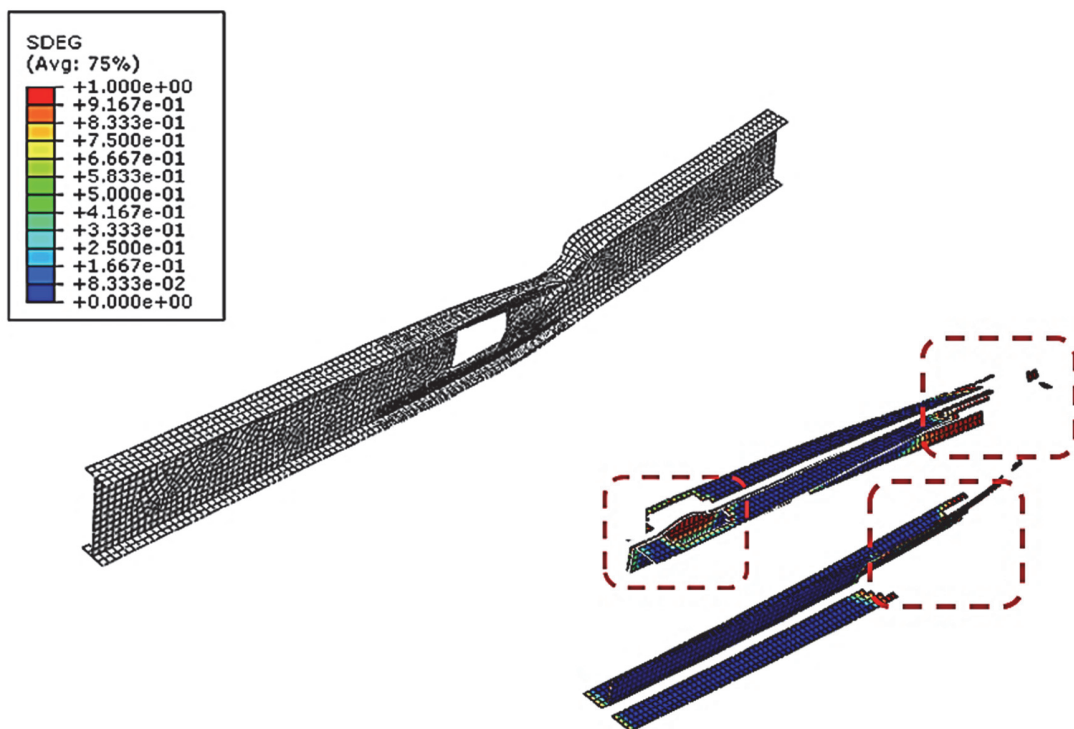


Figure 25: Bond behavior of specimen B1-R1-10.

Shear zone position results

GFRP laminates of 3mm thicknesses

The existence of a large rectangular perforation in the shear zone of the control specimen B0 reduced the beam's strength by 17%, as seen in Fig.26. The same GFRP reinforcement arrangement that was employed for the mid span aperture was applied here to push the perforated beam to regain its initial capacity. Fig. 26 show the load-deflection curves of all GFRP reinforced beams. It can be seen that the percentage of strength enhancement in comparison to B2-U0 was 22%, 32 %, 30 % and 35 % for specimens B2-R1-3,B2-R2-3,B2-R3-3 and B2-R4-3 respectively. Even though GFRP plates of 3 mm (B2-R1-3) did not exhibit the same strength enhancement as CFRP plates of 3 mm, all other reinforced specimens displayed a greater strength enhancement than the control beam and the CFRP strengthened specimen (B2-R0). In addition, the stiffness of the initial beam was restored and it was extremely comparable for all strengthened specimens (Fig.26). Nevertheless, all beams displayed a linear rise up to the same yielding load, which was equal to 360 kN. The initiation of stress concentration was not in the same position. For specimen B2-R4-3, the commencement of plastic hinge creation was in the top flange at the mid-span of the beam. As a response, lateral buckling occurred at the mid span between the central lateral support (Fig.27).In contrary specimens B2-R1-3, B2-R2-3 and B2-R3-3 failed by Vierendeel failure mode (Fig.28).Only specimen B2-R4-3, which used GFRP laminates with a thickness of 3 mm, was capable of influencing the stress status of the beam and demonstrating the same failure mechanism as before (HM CFRP strengthening)[18].This emphasizes the need to select the most appropriate strengthening scheme. Additionally, for specimen B1-R4-3, since the failure occurred outside of the strengthening region, GFRP debonding did not occur. While the SDEG clearly shows that debonding which was performed for specimens B1-R1-3, B1-R2-3, and B1-R3-3 (Fig.29).

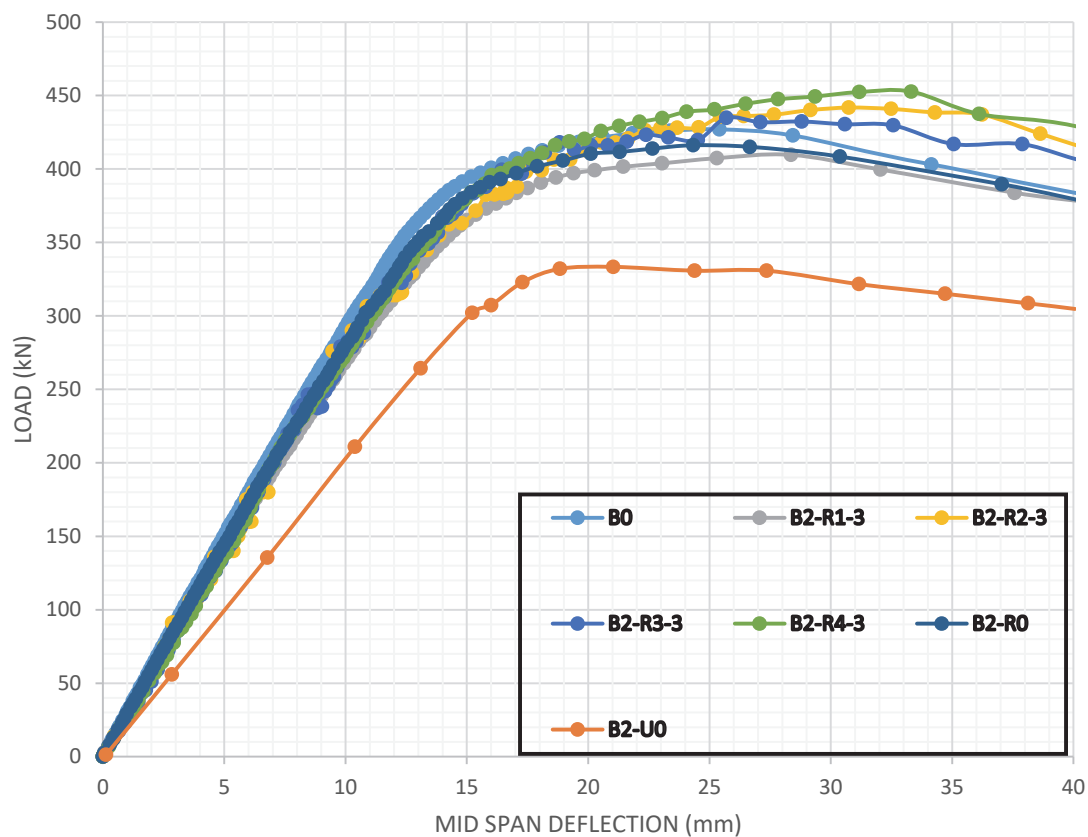


Figure 26: Load deflection curves of specimen B2-U0 strengthened using 3 mm GFRP laminates thicknesses.

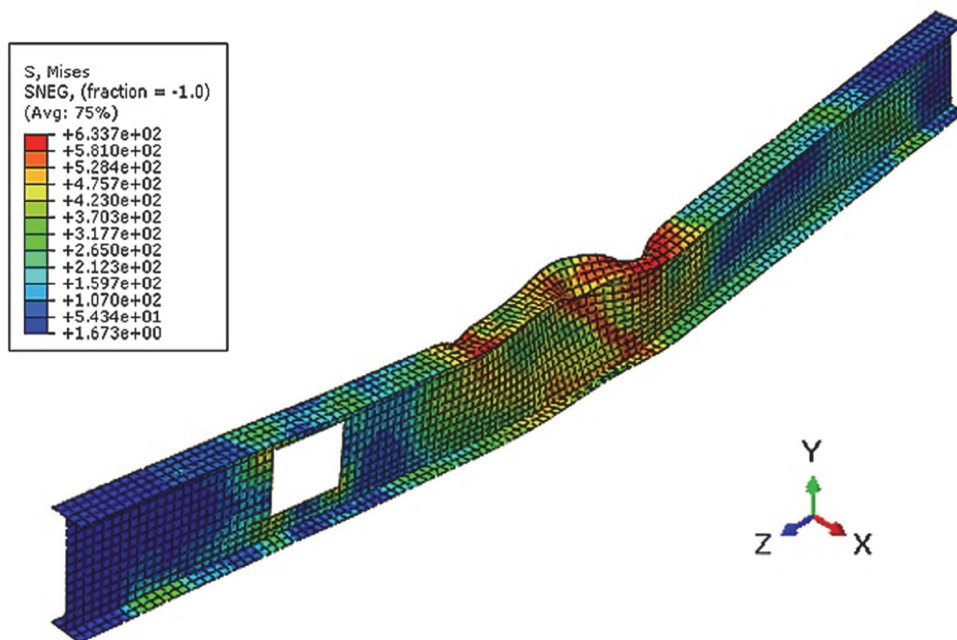


Figure 27: Failure mode for specimen B2-R4-3.

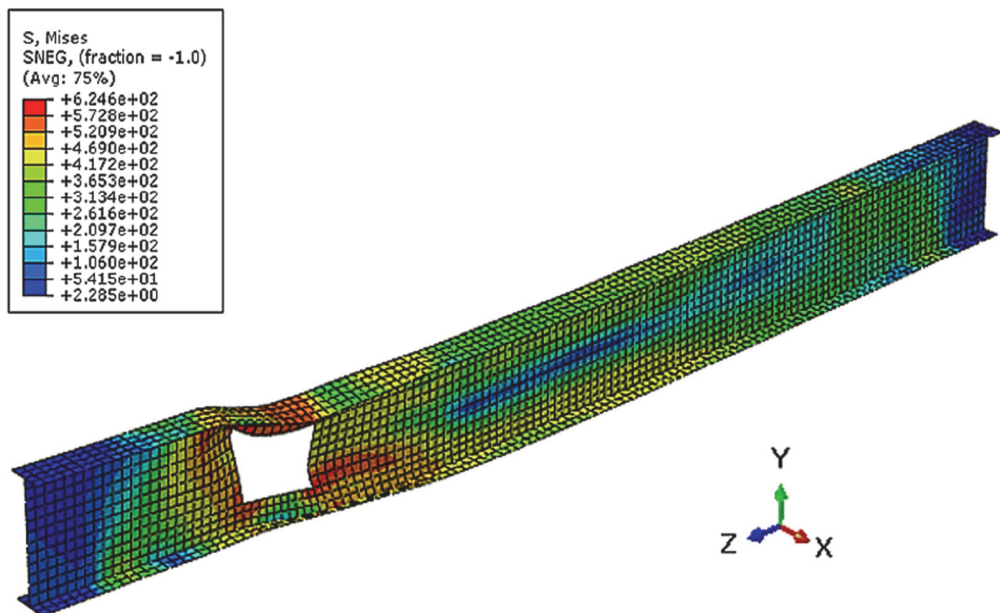


Figure 28: Failure mode for specimen B2-R2-3.

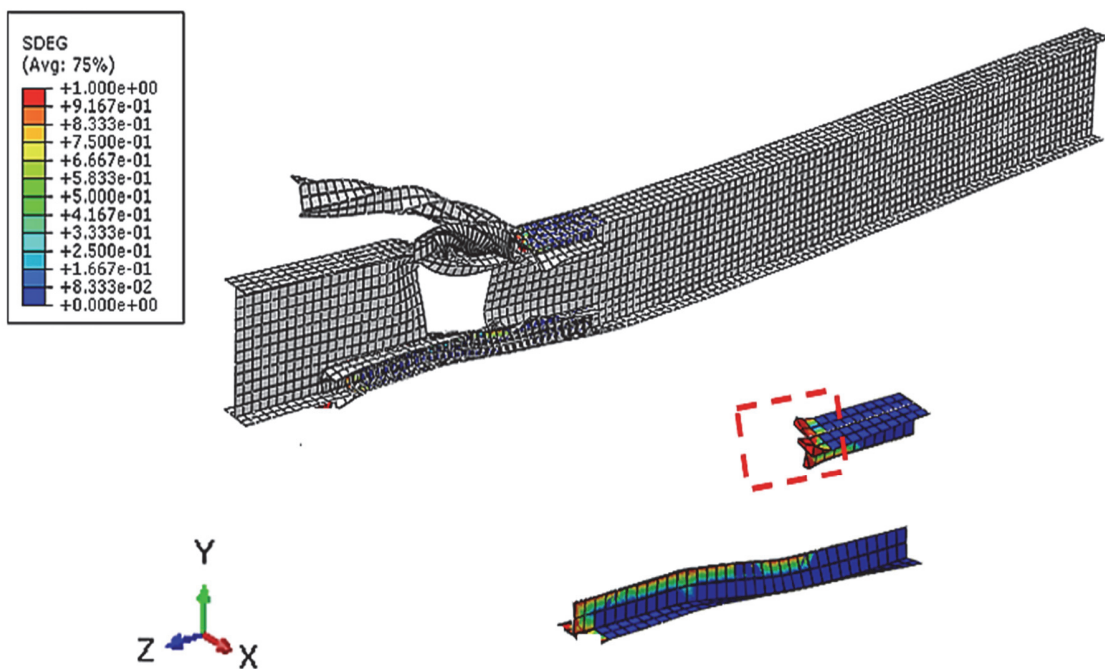


Figure 29: Bond behavior for specimen B2-R2-3.

GFRP laminates of 6mm thicknesses

The prior findings prompted an investigation into the usage of 6mm GFRP laminates. The strength gain varied from 28% to 36% for the GFRP enhanced specimens (Fig.30). The increase of GFRP laminates to 6 mm did not significantly boost the strength improvement in comparison to the previous 3 mm GFRP products. In terms of stiffness, all beams demonstrated remarkably similar stiffness to their original beam B0 when reinforcement was implemented. Up to 360kN of load, all GFRP strengthened beams displayed a linear graph similar to the original and CFRP strengthened beams (B0 and B2-R0). Above this yielding load, the official start of plastic hinge development was in the top flange at the mid-span of all tested specimens. As a reaction, lateral buckling was seen in the specimens' mid span (Fig.31). However, even though the failure mode of all reinforced specimens was outside the strengthened portion, the bond behavior varied. Debonding was detected for examples B2-R2-6 and B2-R3-6, which might be attributable to the lack of bonded GFRP laminates in the beams' bottom flanges (Fig.32).

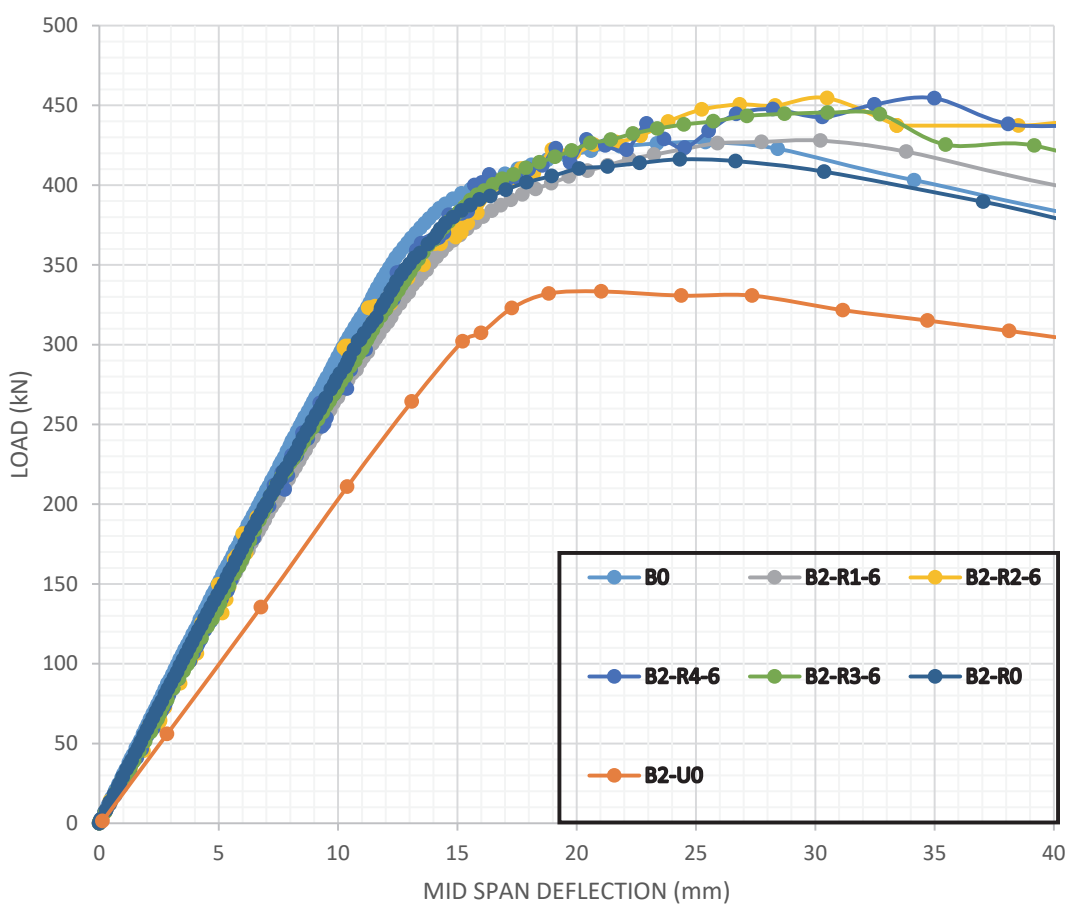


Figure 30: Load deflection curves of specimen B2-UO strengthened using 6 mm GFRP laminates thicknesses.

GFRP laminates of 10 mm thicknesses

As previously reported, the strength gain attained with GFRP thickness increased to 10 mm ranged from 24% to 36% (Fig.33), which indicates that the strength of the initial beam was also restored. In the other hand these findings implies that the increase in GFRP laminate thickness seemed to have no influence on strength and stiffness improvement. This is explained by the premature debonding that occurs before the GFRP reinforcing ability is accomplished, which was the same observation in the previous study with HM CFRP [17]. In contrast to the mid span opening location, even though the augmentation of GFRP laminates to 10 mm did not produce the anticipated strength improvement, it was able to achieve better stiffness for all tested beams, particularly the 'R4' strengthening arrangement. The failure mode of specimens B2-R1-10, B2-R3-10 and B2-R4-10 was changed to mid span later torsional buckling (Fig.34), whereas B2-R2-10 failed by Vierendeel failure mode. In addition to that, debonding was observed with all GFRP strengthened specimens (Fig.35).

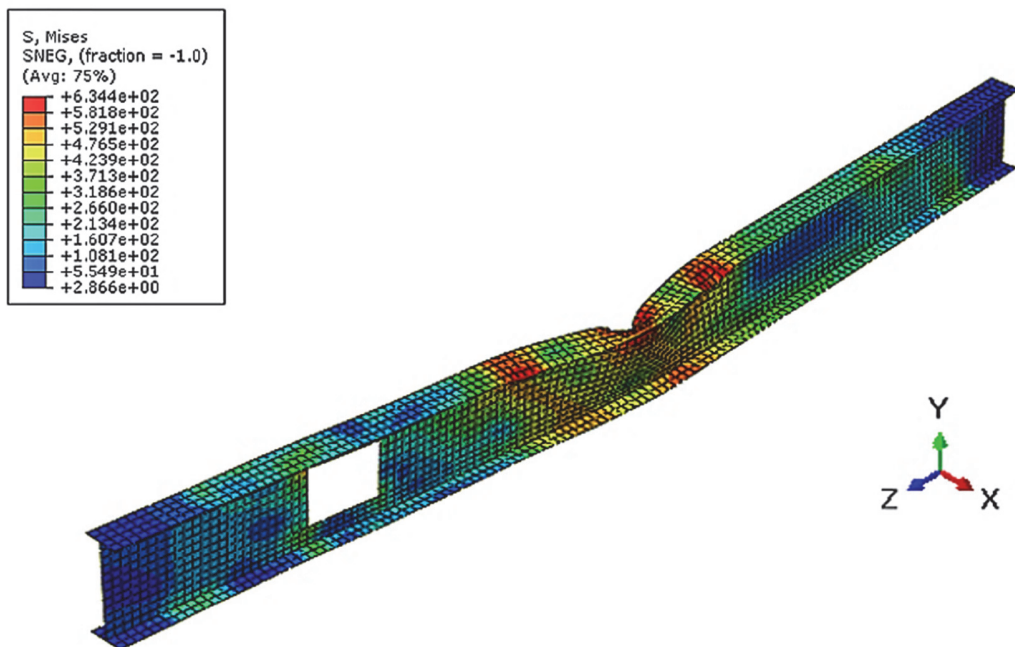


Figure 31: Failure mode for specimen B2-R2-6.

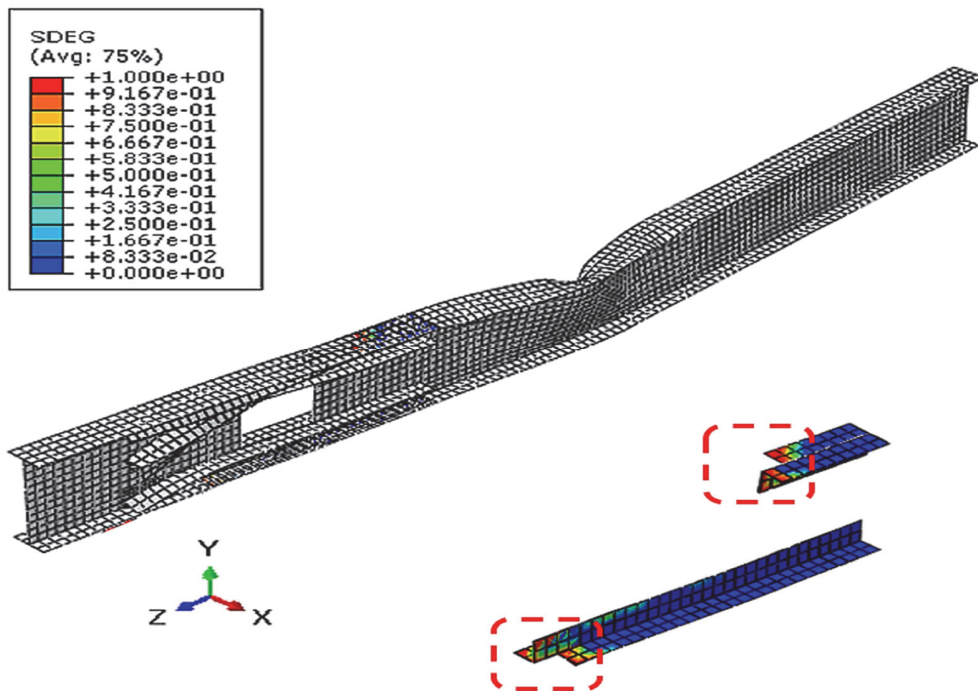


Figure 32: Bond behavior for specimen B2-R2-6.

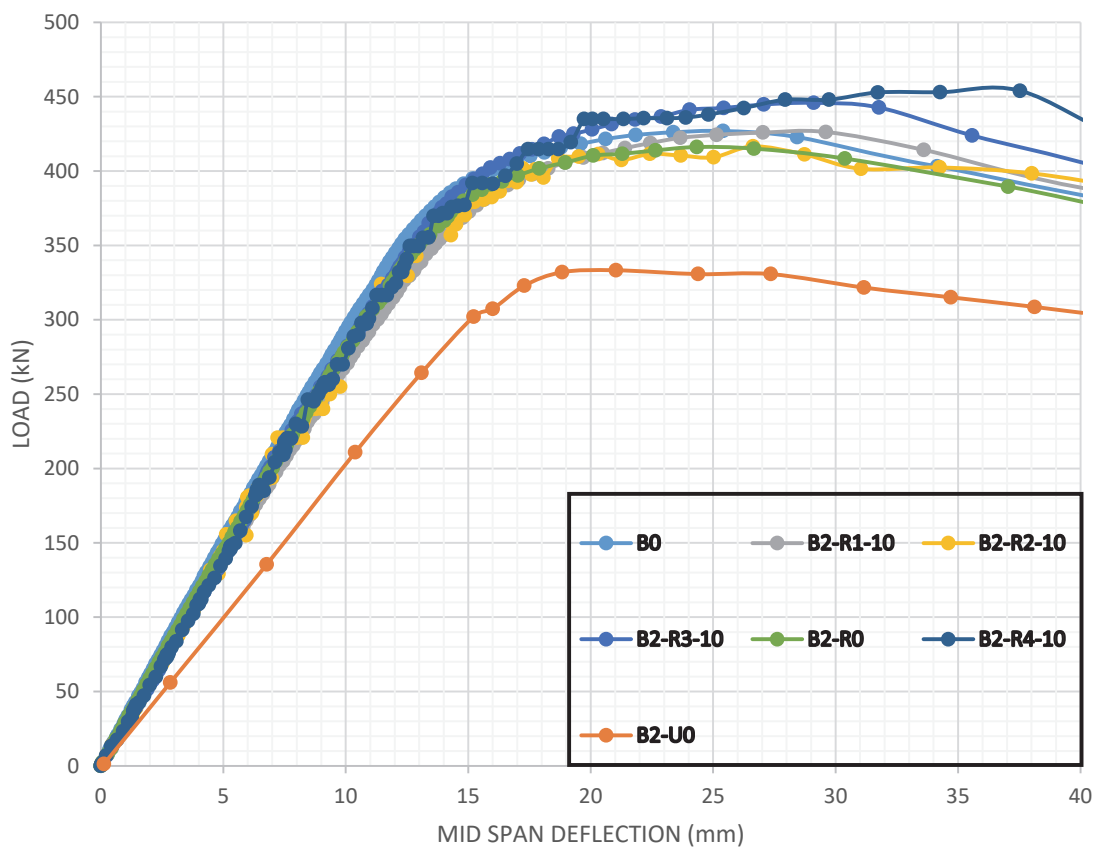


Figure 33: Load deflection curves of specimen B2-U0 strengthened using 10 mm GFRP laminates thicknesses.

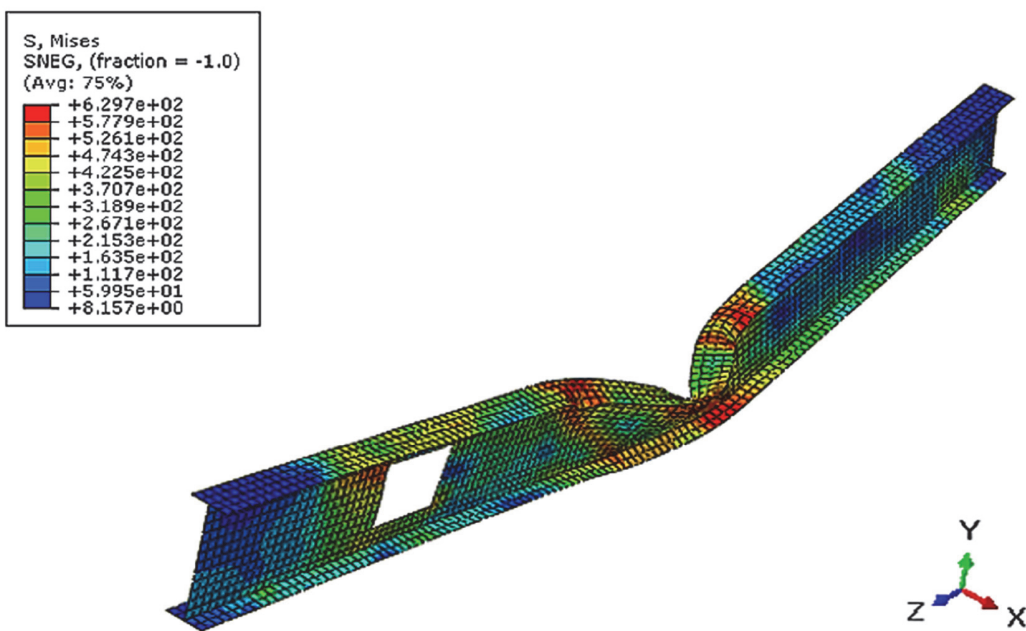


Figure 34: Failure mode of specimen B2-R4-10.

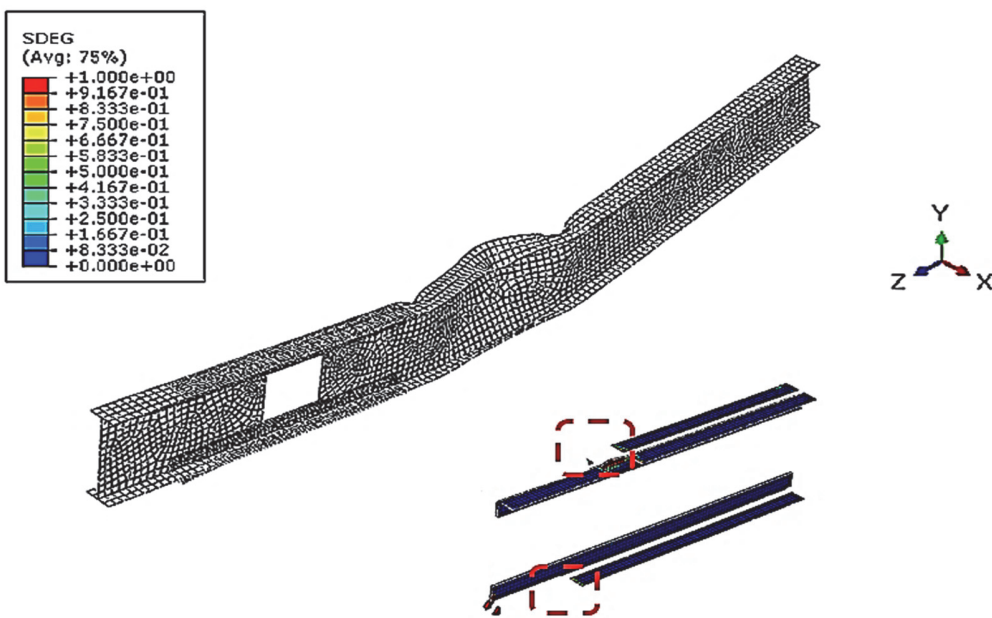


Figure 35: Bond behavior for specimen B2-R1-10.

CONCLUSIONS

In terms of economics, and based on previous results obtained on strengthening steel beams with web openings using CFRP, this study investigated the ability of alternative composites such as GFRP to reinforce web openings in order to gather more information about the use of FRP composites to strengthen these types of beams and progress to a stage where guidelines can be established to support designers in their practical engineering and execution. It was determined that:

- Instead, to CFRP the GFRP strengthening technique proves to be an effective approach in practice for recovering the stiffness and strength of steel beams with rectangular web openings.
- This approach not only assisted to restoring the beam's capacity, but it also provided a boost of strength over to the original solid beam.
- In all situations, the reinforced beams had a stiffer reaction and a higher load-bearing capacity than the unreinforced specimens with web openings.
- The most effective GFRP strengthening technique was the combination of pultruded GFRP T section and plates denoted "R4" in this study.
- The most efficient GFRP thickness for the two web opening positions along the span used in this research was 6 mm, which is equivalent to $0.85 t_w$ and t_f .
- The end debonding, which was noticed in the simulation for the majority of midspan and shear zone opening locations, happened after steel yielding and after the strength recovery.
- Using Araldite 420 epoxy adhesive, this strategy achieves full composite action between steel and GFRP.
- The failure location and mechanism of the strengthened beams were not always the same as in the control or the un-strengthened cases due to this approach of reinforcing.
- The bond length of the CFRP plate layout was suitable for GFRP reinforcing arrangements, particularly configurations "R1" and "R4".
- This finding suggests that GFRP is a suitable, practical and economic way of strengthening steel beams with web openings in comparison to the relatively expensive CFRP.



REFERENCES

- [1] Altaee, M., Cunningham, L., Gillie, M. (2016). CFRP strengthening of steel beams with web openings. In M. C. Forde (Ed.), *Proceedings of Structural Faults & Repair 2016: 16th International Conference*, University of Manchester, UK, p. 1754.
- [2] Elsawaf, S. (2017). Behaviour of structural subassemblies of steel beam with opening, *Civ. Eng. Res. Mag. CERM*, 39(2), pp. 208–27.
- [3] Darwin, D. (2000). Design of composite beams with web openings, *Prog. Struct. Eng. Mater.*, 2(2), pp. 157–63.
- [4] Lawson, R.M., Hicks, S.J. (2011). *Design of Composite Beams with Large web openings*, CSI, Sliwood Park, Ascot, Berkshire, UK.
- [5] Shaker, F.M.F., Shahat, M. (2015). Strengthening of web opening in non-compact steel girders, *IOSR J. Mech. Civ. Eng. e-ISSN*, 12(5), pp. 34–47, DOI: 10.9790/1684-12523447.
- [6] Al-Thabhwhee, H.W.A. (2017). Strengthening Circular Holes in Web of Steel I-Beams, *J. Univ. Babylon*, 25(2), pp. 464–478.
- [7] Cyril Thomas, A., Baskar, K. (2018). Strengthening of thin-webbed castellated beam using CFRP, *Int. J. Comput. Methods Eng. Sci. Mech.*, 19(6), pp. 396–404, DOI: 10.1080/15502287.2018.1534153.
- [8] Zhao, X.L., Zhang, L. (2007). State-of-the-art review on FRP strengthened steel structures, *Eng. Struct.*, 29(8), pp. 1808–1823, DOI: 10.1016/j.engstruct.2006.10.006.
- [9] Narmashiri, K., Ramli Sulong, N.H., Jumaat, M.Z. (2011). Flexural strengthening of steel I-beams by using CFRP strips, *Int. J. Phys. Sci.*, 6(7), pp. 1620–1627, DOI: 10.5897/IJPS11.140.
- [10] Ardalani, G.T., Showkati, H., Teymourlouei, H.E., Firouzsalari, S.E. (2017). The performance of plate girders reinforced with CFRP plates of various lengths, *Thin-Walled Struct.*, 120, pp. 105–115, DOI: 10.1016/j.tws.2017.08.015.
- [11] Deng, J., Lee, M.M.K. (2007). Behaviour under static loading of metallic beams reinforced with a bonded CFRP plate, *Compos. Struct.*, 78(2), pp. 232–242, DOI: 10.1016/j.compstruct.2005.09.004.
- [12] Johnson, T. (2020). *Understanding CFRP Composites*, ThoughtCo, pp. 820393.
- [13] Okeil, A.M., Bingol, Y., Ferdous, M.R. (2009). Novel Technique for Inhibiting Buckling of Thin-Walled Steel Structures Using Pultruded Glass FRP Sections, *J. Compos. Constr.*, 13(6), pp. 547–557, DOI: 10.1061/(ASCE)CC.1943-5614.0000034.
- [14] El Damatty, A.A., Abushagur, M., Youssef, M.A. (2003). Experimental and analytical investigation of steel beams rehabilitated using GFRP sheets, *Steel Compos. Struct.*, 3(6), pp. 421–438, DOI: 10.12989/scs.2003.3.6.421.
- [15] Accord, N.B., Earls, C.J. (2006). Use of Fiber-Reinforced Polymer Composite Elements to Enhance Structural Steel Member Ductility, *J. Compos. Constr.*, 10(4), pp. 337–344, DOI: 10.1061/(ASCE)1090-0268(2006)10:4(337).
- [16] Teng, J.G., Fernando, D., Yu, T. (2015). Finite element modelling of debonding failures in steel beams flexurally strengthened with CFRP laminates, *Eng. Struct.*, 86, pp. 213–224, DOI: 10.1016/j.engstruct.2015.01.003.
- [17] Altaee, M., Cunningham, L.S., Gillie, M. (2019). Practical Application of CFRP Strengthening to Steel Floor Beams with Web Openings: A numerical Investigation, *J. Constr. Steel Res.*, 155, pp. 395–408, DOI: 10.1016/j.jcsr.2019.01.006.
- [18] Altaee, M.J., Cunningham, L.S., Gillie, M. (2017). Experimental investigation of CFRP-strengthened steel beams with web openings, *J. Constr. Steel Res.*, 138, pp. 750–760, DOI: 10.1016/j.jcsr.2017.08.023.
- [19] Mustafa, S.A., Fathy, E., Rizk, M.S. (2020). Fiber-reinforced polymer plates for strengthening web opening in steel I-beams under cyclic loading, *Adv. Struct. Eng.*, 23(2), pp. 348–359, DOI: 10.1177/1369433219868073.
- [20] Hamood, M., Abdulsahib, W., Abdullah, A. (2018). The effectiveness of CFRP strengthening of steel plate girders with web opening subjected to shear. *MATEC Web of Conferences*, 162, EDP Sciences.
- [21] Bouchikhi, A.S., Lousdad, A., Yassine, K., Bouida, N., Gouasmi, S., Megueni, A. (2019). Finite Element Analysis of Interactions of between two cracks in FGM notched Plate under Mechanical Loading, *Frat. Ed Integrità Strutt.*, 13(48), pp. 174–192, DOI: 10.3221/IGF-ESIS.48.20.
- [22] Sahli, A., Merabbi, F., Lousdad, A., Megueni, A. (2020). Optimization design based approach for the determination and minimization of the displacement under tensile load in hybrid composite joint, *Frat. Ed Integrità Strutt.*, 14(52), pp. 281–298, DOI: 10.3221/IGF-ESIS.52.22.
- [23] Farid, B., Boutagouga, D. (2021). Parametric study of I-shaped shear connectors with different orientations in push-out test, *Frat. Ed Integrità Strutt.*, 15(57), pp. 24–39, DOI: 10.3221/IGF-ESIS.57.03.
- [24] Kouider, N., Hadidane, Y., Benzerara, M. (2021). Numerical investigation of the cold-formed I-beams bending strength with different web shapes, *Frat. Ed Integrità Strutt.*, 16(59), pp. 153–171, DOI: 10.3221/IGF-ESIS.59.12.



- [25] ABAQUS.(2013). Theory Manual, User Manual and Example Manual Version 6., Dassault Systemes Simulia Corp.
- [26] Swinnen, J. (2018). Modelling FRP open-hole tensile tests in Abaqus. Delft University of Technology, DOI: 10.1061/(ASCE)CC.1943-5614.0000034.
- [27] Zeng, J.-J., Gao, W.-Y., Liu, F. (2018). Interfacial behavior and debonding failures of full-scale CFRP-strengthened H-section steel beams, Compos. Struct., 201, pp. 540–552, DOI: 10.1016/j.compstruct.2018.06.045.
- [28] Cecchi, A., Russo, S., Sciarretta, F. (2017). Preliminary Investigation on FRP Profiles for the Structural Retrofit of Masonry Structures, Key Eng. Mater., 747, pp. 77–84, DOI: 10.4028/www.scientific.net/KEM.747.77.
- [29] Guedaoura, H., Hadidane, Y. (2022). Web post-buckling strength of thin-webbed cellular beams using carbon PFRP profiles, Frat. Ed Integrità Strutt., 16(60), pp. 43–61, DOI: 10.3221/IGF-ESIS.60.04.

NOMENCLATURE

- GFRP : Glass fiber reinforced polymer.
- CFRP : Carbon fiber reinforced polymer.
- BFRP : Basalt fiber reinforced polymer.
- E : Elastic modulus of steel.
- f_y : Yield stress.
- ϵ_{true} : True strain.
- $\epsilon_{\text{nominal}}$: Nominal strain.
- σ_{true} : True stress.
- σ_{nominal} : Nominal stress.
- E_x : Elastic modulus in the fiber direction.
- E_y, E_z : Elastic modulus in the transverse direction.
- G_{xy} : In-plane shear modulus.
- G_{xz}, G_{yz} : Shear modulus in the transverse direction.
- ν : Poisson ratio.
- b_f : Flange width.
- t_f : Flange thickness.
- t_w : Web thickness.
- H : height of profile.
- L : Length of the beam.
- P_u : Ultimate load.
- D : The scalar damage variable.
- K_{nn} : The adhesive elastic stiffness in the normal direction, which is equal to the initial slope of the bond-separation model for mode-I loading.
- K_{ss} and K_{tt} : The adhesive elastic stiffness in the shear directions.
- E_a : Elastic modulus of the adhesive layer.
- G_a : The shear module of the adhesive layer.
- T_a : Thickness of the adhesive layer.
- δ_n, δ_s and δ_t : Separations in the corresponding directions.
- σ_{\max} : The peak stress in the normal direction.
- τ_{\max} : The peak stress in the shear directions.
- t_n, t_s and t_t : The peak stresses in the normal and two shear directions.



δ_m^{\max} :	The maximum effective relative displacement attained during the loading history.
δ_m^0, δ_m^f :	The effective relative displacement at the initiation and end of failure respectively.
<i>SDEG</i> :	Stress degradation parameter.
<i>TFY</i> :	Top flange yielding.
<i>LTB</i> :	Lateral torsional buckling.
<i>DEB</i> :	Debonding.